J. Fluid Mech. (2001), *vol.* 427, *pp.* 167–204. Printed in the United Kingdom

Quasi-one-dimensional steady-state cavitating nozzle flows

By C. F. DELALE[1], G. H. SCHNERR[2] AND J. SAUER[2]

[1]TÜBİTAK Feza Gürsey Institute, P.O. Box 6, 81220 Çengelköy, Istanbul, Turkey

[2]Fachgebiet Strömungsmaschinen, Universität Karlsruhe (TH), Kaiserstrasse 12, D-76128 Karlsruhe, Germany

(Received 21 September 1998 and in revised form 8 August 2000)

Quasi-one-dimensional cavitating nozzle flows are considered by employing a homogeneous bubbly liquid flow model. The nonlinear dynamics of cavitating bubbles is described by a modified Rayleigh–Plesset equation that takes into account bubble/bubble interactions by a local homogeneous mean-field theory and the various damping mechanisms by a damping coefficient, lumping them together in the form of viscous dissipation. The resulting system of quasi-one-dimensional cavitating nozzle flow equations is then uncoupled leading to a nonlinear third-order ordinary differential equation for the flow speed. This equation is then cast into a nonlinear dynamical system of scaled variables which describe deviations of the flow field from its corresponding incompressible single-phase value. The solution of the initial-value problem of this dynamical system can be carried out very accurately, leading to an exact description of the hydrodynamic field for the model considered.

A bubbly liquid composed of water vapour–air bubbles in water at 20°C for two different area variations is considered, and the initial cavitation number is chosen in such a way that cavitation can occur in the nozzle. Results obtained, when bubble/bubble interactions are neglected, show solutions with flow instabilities, similar to the flashing flow solutions found recently by Wang and Brennen. Stable steady-state cavitating nozzle flow solutions, either with continuous growth of bubbles or with growth followed by collapse of bubbles, were obtained when bubble/bubble interactions were considered together with various damping mechanisms.

1. Introduction

Hydrodynamic cavitation, i.e. formation of bubbles by incipient nucleation followed by the growth and collapse structures of bubbles in a flowing liquid, is a formidable problem. The subject matter arises in many engineering applications such as cavitation in hydraulic machinery, the flow around a cavitating hydrofoil or propeller blade, etc. It is also of considerable interest in physics, chemistry and biology because of the various phenomena that arise owing to the growth and collapse of bubbles. The subject is most frequently investigated experimentally; however, it is usually difficult to transfer data obtained from a model in an experimental facility to real size. Sometimes, it may even be difficult to compare results of identical experimental configurations (e.g. see Knapp, Daily & Hammitt 1970; Hammitt 1980; Young 1989). Thus, hydrodynamic cavitation can be taken to be unsteady and statistical in nature. For this reason, it is usual to consider simplified models, which are often solvable numerically, to gain some understanding about the phenomena. Cavitating flows in ducts and in converging–diverging nozzles seem to be the simplest configurations for analysis.

Nozzle flow characteristics for isothermal frictionless bubbly flow of a barotropic mixture were first considered by Tangren, Dodge & Seifert (1949) and a discussion of such flows can be found in the works of Wallis (1969), van Wijngaarden (1972) and, more recently, Brennen (1995). Steady flows of bubbly liquids through a converging-diverging nozzle have also recently been considered by Ishii *et al.* (1993) by assuming that the gas pressure inside the bubble is the same as the ambient fluid pressure (there, bubble dynamics is neglected). For cavitating nozzle flows it is essential to consider bubble dynamics together with the equations of nozzle flow. A homogeneous two-phase bubbly mixture model that couples spherical bubble dynamics, as described by the classical Rayleigh–Plesset equation, to the flow equations was proposed by van Wijngaarden (1968, 1972) and was used for investigating shock wave structure in bubbly liquids (e.g. see Noordzij & van Wijngaarden 1974; Kameda & Matsumoto 1995). Schulz (1995; also briefly discussed in Schnerr *et al.* 1995) has considered cavitating nozzle flows in one and two dimensions in this model with and without bubble/flow interactions using a numerical method. Only recently have Wang & Brennen (1997, 1998) used this model to investigate numerically bubble/flow interactions of cavitating flows in a converging–diverging nozzle using real fluid properties and considering damping mechanisms by a damping coefficient in the form of viscous dissipation. Their results show that bubble/flow interactions have important effects on the confined flow field. They consider steady flow, and find two different flow regimes: a quasi-statically unstable flow, which they call flashing flow; and a quasi-statically stable flow with a ringing structure of growth and collapse of bubbles downstream of the throat.

The purpose of this investigation is to analyse quasi-one-dimensional cavitating nozzle flows by constructing a model with spherical bubble dynamics. For this reason, a modified Rayleigh–Plesset equation that takes into account bubble/bubble interactions by a slightly modified local homogeneous model of Kubota, Kato & Yamaguchi (1992) and that treats the various damping effects, by lumping them together in the form of viscous damping by a damping coefficient, is derived. The ambient pressure of the bubbles is set equal to the local value of the mixture pressure (see van Wijngaarden 1968). The resulting system of the model equations is then uncoupled and a nonlinear third-order ordinary differential equation for the flow speed is obtained. By appropriate scaling, this equation is cast into a nonlinear dynamical system of scaled variables which represent deviations of the flow speed and its derivatives from their incompressible single-phase values. The solution of the initial-value problem of this dynamical system then leads to the exact solution of quasi-one-dimensional cavitating nozzle flows in this model.

A bubbly liquid composed of water vapour–air bubbles in water at 20°C with two different area variations is considered and the initial cavitation number is chosen in such a way that cavitation can occur in each nozzle. Results obtained when bubble/bubble interactions are neglected show stable solutions with limited growth and collapse of bubbles (stable non-cavitating flows) with maximum radius smaller than the Blake radius, as reasoned in appendix C, for certain values of the specified parameters. For most of the cases investigated without taking into account-bubble/bubble interactions, the initial-value problem of the model equations leads to blow-up solutions with flow instabilities. These instabilities can be overcome by taking into account bubble/bubble interactions and various damping effects simultaneously leading to stable steady-state cavitating nozzle flow solutions either with continuously growth of bubbles or with growth of bubbles followed by collapse at the nozzle exit.

2. Model equations for quasi-one-dimensional cavitating nozzle flows

We consider the quasi-one-dimensional cavitating flow of a bubbly liquid through a converging–diverging nozzle with axial coordinate x' and cross-sectional area $A'(x')$, as shown in figure 1. We use the averaged equations for a bubbly flow (van Wijngaarden 1968; Wang & Brennen 1998), the averages being carried out in a volume with mesoscopic lengthscale containing many bubbles centred about the macroscopic position (for details see Biesheuvel & van Wijngaarden 1984). Moreover, all bubbles inside this volume are assumed to be spherical in shape with the same bubble radius R'. We assume steady flow, a constant viscosity model for the mixture and no slip between the phases. The quasi-one-dimensional nozzle flow equations for such a mixture then take the form (e.g. see Wang & Brennen 1997, 1998)

$$\rho' = \rho'_\ell\,(1-\beta), \tag{1}$$

$$\rho'\,u'\,A' = \text{constant}, \tag{2}$$

$$\rho'\,u'\,\frac{\mathrm{d}u'}{\mathrm{d}x'} = -\frac{\mathrm{d}p'}{\mathrm{d}x'} + \tfrac{4}{3}\mu'_m\frac{\mathrm{d}^2u'}{\mathrm{d}x'^2} - \frac{\mathscr{P}'}{A'}\,\tau'_w \tag{3}$$

and

$$\beta = \frac{\frac{4}{3}\pi R'^3\,n'_0}{1+\frac{4}{3}\pi R'^3\,n'_0} = \tfrac{4}{3}\pi R'^3\,N'. \tag{4}$$

In the above equations p', ρ', u' and β are, respectively, the mixture pressure, the mixture density, the mixture velocity and the void fraction, ρ'_ℓ is the liquid density (assumed to be constant), μ'_m is the mixture viscosity (herein taken as the same as the liquid viscosity μ'_ℓ), R' is the bubble radius, $\mathscr{P}'$ is the wetted perimeter of the nozzle (for a plane two-dimensional nozzle $\mathscr{P}'$ is twice the depth of the nozzle), τ'_w is the absolute value of the wall shear stress, N' is the concentration of bubbles per unit volume of the mixture and n'_0 is the conveniently defined concentration of bubbles per unit volume of flowing liquid. In particular n'_0 is related to N' by

$$n'_0 = \frac{N'}{1-\beta} = \text{constant}. \tag{5}$$

Equation (1) simply relates the mixture density ρ' to the void fraction β in the homogeneous flow model where it is implicit that $\rho'_i/\rho'_\ell \ll 1$ with ρ'_i denoting the density of the bubble content (gaseous phase plus vapour). Equation (2) is the conservation of mass in steady nozzle flows whereas (3) is the momentum equation in a nozzle with internal viscous dissipation and wall friction (e.g. see Wallis 1969). Equation (4) defines the void fraction (e.g. see Brennen 1995). The above equations (1)–(4) do not form a closed system unless they are supplemented by a microscopic equation for bubble dynamics.

2.1. *Spherical bubble dynamics: a modified Rayleigh–Plesset equation*

A model for spherical bubble dynamics that couples the classical Rayleigh–Plesset equation to equations (1)–(4) was first proposed by van Wijngaarden (1968, 1972) and it has recently been employed by Wang & Brennen (1997, 1998) to investigate cavitating flows through a convergent–divergent nozzle. In this model, each bubble grows and collapses independently according to the classical Rayleigh–Plesset equation

$$\frac{p'_i - p'}{\rho'_\ell} = R'\,\frac{\mathrm{d}^2R'}{\mathrm{d}t'^2} + \frac{3}{2}\left(\frac{\mathrm{d}R'}{\mathrm{d}t'}\right)^2 + \frac{2\,S'}{\rho'_\ell\,R'} + \frac{4\,v'_D}{R'}\,\frac{\mathrm{d}R'}{\mathrm{d}t'}, \tag{6}$$

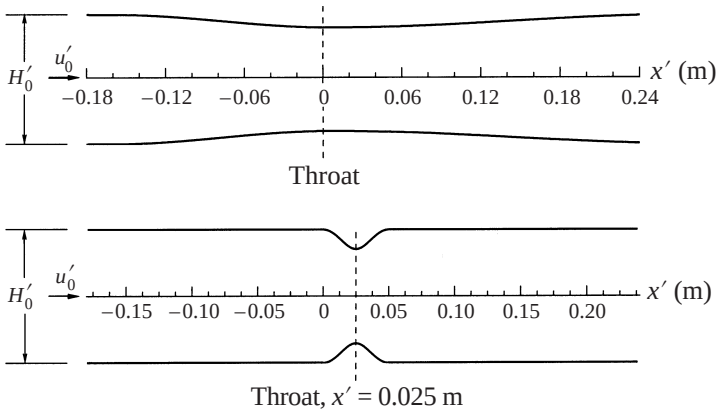

FIGURE 1. Investigated nozzle geometries. Top: nozzle 1 investigated by Schulz (equation (86)). Bottom: nozzle 2 investigated by Wang & Brennen (equation (87)).

where S' is the surface tension coefficient, p_i' is the total bubble pressure (assumed to be uniform throughout the bubble), $\mathrm{d}/\mathrm{d}t'$ denotes the total or material derivative which reduces to $u'\,\mathrm{d}/\mathrm{d}x'$ for steady flow and where the ambient pressure is set equal to the local pressure p'. In (6), all of the damping mechanisms are lumped together and represented by a single damping coefficient $\nu_D' = \mu_D'/\rho_\ell'$ with μ_D' replacing the liquid viscosity μ_ℓ'. It can be argued that the introduction of the single coefficient ν_D' in (6) to represent all of the damping mechanisms in the form of viscous damping is an *ad hoc* assumption. As will be discussed in detail below, such a simplification does not only stem from trying to achieve simplicity in analysis and computations, but is also due to the lack of satisfactory knowledge of damping mechanisms (besides viscous damping) for cavitating bubbles. Assuming that the bubble contains a contaminant gas with partial pressure p_g' together with the vapour with partial pressure p_v', the total bubble pressure p_i' can be taken as the sum of the partial pressures of the gas and vapour (an ideal mixture of gases). With these in mind, the behaviour of the gas in the bubble can be taken to be polytropic so that

$$p_i' = p_v' + p_g' = p_v' + p_{g0}' \left(\frac{R_0'}{R'}\right)^{3k}, \tag{7}$$

where k is the polytropic index ($k = 1$ implies a constant bubble temperature whereas $k = \gamma$, with γ denoting the isentropic exponent of the gas, would model isentropic gas behaviour), R_0' is the initial radius of bubbles at the nozzle inlet and p_{g0}', which in our case will be fixed by the mechanical equilibrium condition at the nozzle inlet, is the initial partial gas pressure.

It has recently been shown by Wang & Brennen (1997, 1998) that van Wijngaarden's equations, given by (1)–(7) above, lead to flow instabilities in cavitating nozzle flows for their chosen values of the damping coefficient ν_D'. Therefore, the ramification of these instabilities has to be considered by modifying (6) for bubble dynamics. This ramification should include bubble/bubble interactions, non-spherical bubble shape, liquid compressibility and additional damping mechanisms such as thermal behaviour of bubbles, acoustic radiation, etc. The simplified model, given above by (1)–(7), neglects completely the effects of bubble/bubble interactions, non-spherical bubble shape and liquid compressibility and it takes into account the effects of various damping mechanisms by the single coefficient ν_D'. It is well known that spherical bubble

dynamics is violated near boundaries (e.g. see Blake & Gibson 1987) and that liquid compressibility can be significant in the collapse period (e.g. see Prosperetti & Lezzi 1986). For quasi-one-dimensional nozzle flows to be investigated herein, we will leave out these effects to avoid complications in analysis with the expectation that these effects will be secondary compared to those of bubble/bubble interactions and various damping mechanisms. Therefore, we will modify (6) and (7) taking into account the latter effects only. It is also worthwhile to note that the investigation of Chahine & Duraiswami (1992) has shown that bubble/bubble interactions in a multi-bubble cloud inhibit bubble growth while they enhance bubble collapse. Consequently, in modifying (6) and (7), bubble/bubble interactions and various damping mechanisms have to be considered separately.

In this study, we first employ the local homogeneous model introduced by Kubota *et al.* (1992) to model bubble/bubble interactions. In this model bubble/bubble interactions are taken into account within spherical bubbly clusters, each of radius $\Delta r'$, as shown in figure 2. The total velocity potential at the centre O of a cluster resulting from interactions with other bubbles within the cluster is

$$\sum_i \left(\frac{1}{r_i'} R_i'^2 \frac{\mathrm{d}R_i'}{\mathrm{d}t'} \right), \tag{8}$$

where it is understood that the summation is carried out over all bubbles interacting with the one at the centre. In (8), R_i' is the radius of a bubble at a distance r_i' ($\gg R_i'$) from the centre O (see figure 2). Using the local homogeneous assumption

$$\nabla \left(\sum_i \frac{1}{r_i'} R_i'^2 \frac{\mathrm{d}R_i'}{\mathrm{d}t'} \right) = 0, \tag{9}$$

and assuming that all bubbles within the spherical cluster have the same radius R', the Rayleigh–Plesset equation (6) can be modified as

$$\frac{p_i' - p'}{\rho_\ell'} = \frac{\mathrm{d}}{\mathrm{d}t'} \left(R'^2 \frac{\mathrm{d}R'}{\mathrm{d}t'} \sum_i \frac{1}{r_i'} \right) + R' \frac{\mathrm{d}^2 R'}{\mathrm{d}t'^2} + \frac{3}{2} \left(\frac{\mathrm{d}R'}{\mathrm{d}t'} \right)^2 + \frac{2S'}{\rho_\ell' R'} + \frac{4 v_D'}{R'} \frac{\mathrm{d}R'}{\mathrm{d}t'}, \tag{10}$$

to include bubble/bubble interactions in the model considered. By noting that the number of bubbles interacting with the bubble at the centre inside a cluster of radius $\Delta r'$ is

$$\tfrac{4}{3}\pi N' \left[(\Delta r')^3 - R'^3 \right], \tag{11}$$

the first term on the right-hand side of (10) can be written as

$$\begin{aligned} \frac{\mathrm{d}}{\mathrm{d}t'} \left(R'^2 \frac{\mathrm{d}R'}{\mathrm{d}t'} \sum_i \frac{1}{r_i'} \right) &\approx \frac{\mathrm{d}}{\mathrm{d}t'} \left(R'^2 \frac{\mathrm{d}R'}{\mathrm{d}t'} N' \int_{R'}^{\Delta r'} \frac{1}{r'} 4\pi r'^2 \mathrm{d}r' \right) \\ &= \frac{\mathrm{d}}{\mathrm{d}t'} \left(2\pi N' \left[(\Delta r')^2 - R'^2 \right] R'^2 \frac{\mathrm{d}R'}{\mathrm{d}t'} \right). \end{aligned} \tag{12}$$

Until now, $\Delta r'$ has been left arbitrary. At this stage we further assume that

$$\Delta r' = \Lambda R', \tag{13}$$

where $\Lambda = \textit{constant} \gg 1$ (the particular case where $\Lambda = 1$ yields single bubble dynamics without bubble/bubble interactions, as described by the classical Rayleigh–Plesset equation (6)). This assumption implies an interaction model for which the

local number of bubbles within a cluster is proportional to the local volume of a bubble, thereby, to the local void fraction β . This simple model is indeed reasonable since bubble/bubble interactions become more significant for larger values of the void fraction β. By substituting from (5), (12) and (13) into (10), we obtain a modified Rayleigh–Plesset equation as

$$\frac{p_i' - p'}{\rho_\ell'} = \frac{\left[1 + \frac{2}{3}\pi n_0' (3\Lambda^2 - 1) R'^3\right]}{\left[1 + \frac{4}{3}\pi n_0' R'^3\right]} R' \frac{d^2 R'}{dt'^2} + \frac{3}{2} \frac{\left[1 + \frac{8}{3}\pi n_0' (2\Lambda^2 - 1) R'^3 + \frac{16}{9}\pi^2 n_0'^2 \Lambda^2 R'^6\right]}{\left[1 + \frac{4}{3}\pi n_0' R'^3\right]^2} \left(\frac{\mathrm{d}R'}{\mathrm{d}t'}\right)^2 + \frac{2S'}{\rho_\ell' R'} + \frac{4\nu_D'}{R'} \frac{\mathrm{d}R'}{\mathrm{d}t'}, \tag{14}$$

which reduces to the classical Rayleigh–Plesset equation for $\Lambda = 1$, the case where bubble/bubble interactions are completely left out. We now show that the model equation (14) for spherical bubble dynamics, which incorporates bubble/bubble interactions as in the local homogeneous model of Kubota *et al.* (1992), is indeed in qualitative agreement with the well-established result that bubble/bubble interactions inhibit bubble growth, but they enhance bubble collapse (e.g. see Chahine & Duraiswami 1992). We first note that bubble/bubble interactions are most significant in regions near maximum bubble radius where $\mathrm{d}^2R'/\mathrm{d}t'^2 < 0$. The first and second terms on the right-hand side of (14) for $\Lambda \gg 1$ are seen to be modified by the factors $[1 + (1/2)\Lambda^2\beta]$ and $[1 + (4/3)\Lambda^2\beta]$, respectively, to linear order in β as compared to the classical Rayleigh–Plesset equation ($\Lambda = 1$). Consequently, at any location near maximum bubble radius with fixed flow variables, fixed bubble radius R' and fixed bubble growth or collapse velocity $\mathrm{d}R'/\mathrm{d}t'$, the increase in the second term should balance the decrease in the first term on the right-hand side of (14), as compared to the case where bubble/bubble interactions are left out. This implies that, at any location, the absolute value of the radial deceleration $\mathrm{d}^2R'/\mathrm{d}t'^2$ will be greater when bubble/bubble interactions are included. Thus, bubble/bubble interactions, as incorporated in (14), inhibit bubble growth ($\mathrm{d}R'/\mathrm{d}t' > 0$) and enhance bubble collapse ($\mathrm{d}R'/\mathrm{d}t' < 0$).

Having considered bubble/bubble interactions, we now discuss the various damping mechanisms of nonlinear bubble dynamics and show how the single damping coefficient ν_D' in (14) should be interpreted. The most common damping mechanisms include thermal conduction through the gas, viscosity of the liquid and acoustic radiation (bubble fission occurring after the first collapse, as discussed by Colonius, Brennen & d'Auria (1998), should also be included). The problem of thermal conduction through the gas for small-amplitude gas bubbles was considered by Chapman & Plesset (1971, see also the references therein). The problem has been treated rigorously for gas bubbles undergoing nonlinear oscillations by Nigmatulin, Khabeev & Nagiev (1981), Miksis & Ting (1984, 1987), Prosperetti, Crum & Commander (1988) and Prosperetti (1991). All of these investigations consider the energy equation for the gas inside the bubble and solve the coupled system of equations numerically under specified initial and boundary conditions. The results show that there is deviation from the polytropic law of equation (7) demonstrating the strong influence of damping from thermal conduction of the gas on bubble dynamics, which cannot be taken into account by any crude model that avoids the use of the energy equation, in spite of the fact that the uniformity of the gas pressure holds to a good approximation (for low

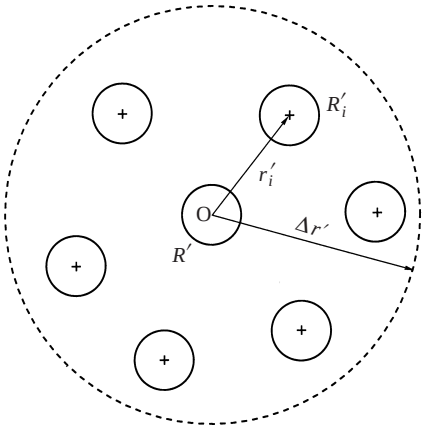

FIGURE 2. Geometric configuration of bubbles for the mean-field bubble/bubble interactions within a radius of influence $\Delta r'$ (R' is the bubble radius at the centre O and R_i' is the radius of the ith bubble located at a distance r_i' from the centre).

bubble wall Mach numbers). In particular, Prosperetti *et al.* (1988) and Prosperetti (1991) have simplified the mathematical formulation of the thermal conduction problem arriving at three coupled differential equations for the temperature, the radial velocity and the pressure of the gas with appropriate initial and boundary conditions. This model has also been applied by Watanabe & Prosperetti (1994) to explain the structure of different types of shock observed in the experiments of Noordzij & van Wijngaarden (1974). As mentioned by Prosperetti *et al.* (1988) and Prosperetti (1991), the application of the model to cavitating bubbles should be taken very cautiously since the model neglects the effects of the vapour within the bubble and assumes that the bubble wall Mach number is small, a condition which may not be fulfilled in the violent collapse stages of cavitating bubbles. Nevertheless, for cold liquids (e.g. for water up to 50°C) vapour effects can be shown to be negligible (see Prosperetti *et al.* 1988). At present, the model seems to be much more promising than a model that uses a polytropic law for the gas behaviour together with a damping cofficient, in the form of viscous dissipation, as in (14). The three differential equations of Prosperetti (1991) for the temperature, the radial velocity and the pressure of the gas within the bubble with appropriate initial and boundary conditions can then be solved simultaneously at each location along the nozzle axis together with (1)–(5), (10) and (14) (in this case the damping coefficient ν_D' of (14) can be assumed to be of the same order of magnitude as that of the kinematic viscosity ν_ℓ' of the liquid). This procedure has to be carried out numerically and can show complications with respect to computation method and computation time and, therefore, it is not convenient for the work to be presented in this paper.

Prosperetti (1991) also considered the limiting cases of near-isothermal ($k = 1$) and near-isentropic ($k = \gamma$) behaviour of the gas and found explicit relations between the modified gas pressure and bubble dynamics. For simplicity, we will only consider the near-isothermal behaviour and modify (7) as

$$p_i' = p_v' + p_g' = p_v' + p_{g0}' \left(\frac{R_0'}{R'}\right)^3 \left[1 - \frac{(\gamma - 1)}{5\gamma} \left(\frac{R_0'}{R'}\right)^2 \frac{R_0'}{\alpha'} \frac{\mathrm{d}R'}{\mathrm{d}t'}\right], \tag{15}$$

where α' is the thermal diffusivity of the gas. It should be mentioned that (15) can

only be employed in the near-isothermal case. In this case, v'_D in (14) will represent all of the damping contributions except those arising from the thermal behaviour of the gas. In this paper, except for the limiting near-isothermal behaviour of (15), we will employ the polytropic law of (7) for the gas behaviour and represent all damping mechanisms lumping them together in the form of viscous dissipation by the damping coefficient v'_D in (14). Despite the fact that the damping mechanisms (except that of viscous damping) lack the correct form for cavitating bubbles in this simplified model, the model will prove useful in furnishing the relative magnitude of the damping effect (with respect to viscous damping) necessary to stabilize the flow towards stable steady-state solutions. Equations (1)–(4) and the modified Rayleigh–Plesset equation (14) together with (7) (or (15) when $k = 1$) constitute the model equations we will use in our investigation of quasi-one-dimensional cavitating nozzle flows.

2.2. *Normalized model equations*

We now normalize the above model equations. For convenience, we define the non-dimensional mixture density ρ, mixture pressure p, partial vapour pressure p_v, partial gas pressure p_g and mixture velocity u by

$$\rho = \frac{\rho'}{\rho'_\ell} = 1 - \beta,\ p = \frac{p'}{p'_0},\ p_v = \frac{p'_v}{p'_0},\ p_g = \frac{p'_g}{p'_0},\ u = \frac{u'}{\sqrt{p'_0/\rho'_\ell}}, \tag{16}$$

where p'_0 is the static pressure at the nozzle inlet. We also normalize the axial coordinate x', the cross-sectional area A' and the bubble radius R' by

$$x = \frac{x'}{H'_0}, \quad A = \frac{A'}{A'_0}, \quad R = \frac{R'}{R'_0}, \tag{17}$$

where H'_0 is the inlet nozzle height as shown in figure 1, A'_0 is the inlet cross-sectional area of the nozzle (for a two-dimensional nozzle it can be taken as the inlet height H'_0) and R'_0 is the initial radius of bubbles (taken as monodispersed). In particular, R'_0 can be related to the inlet void fraction β_0 by

$$\beta_0 = \frac{\frac{4}{3}\pi {R'_0}^3 n'_0}{1 + \frac{4}{3}\pi {R'_0}^3 n'_0}. \tag{18}$$

The quasi-one-dimensional steady nozzle flow equations (1)–(4) together with the modified Rayleigh–Plesset equation (14) and equations (7) and (15) then become

$$\rho = 1 - \beta, \tag{19}$$

$$\rho u A = \lambda_0 = (1 - \beta_0) u_0, \tag{20}$$

$$\rho u \frac{\mathrm{d}u}{\mathrm{d}x} = -\frac{\mathrm{d}p}{\mathrm{d}x} + \frac{4}{3\,(Re_\ell)} \frac{\mathrm{d}^2 u}{\mathrm{d}x^2} - \varphi C_w \rho u^2, \tag{21}$$

$$R = \kappa_0 \left(\frac{\beta}{1 - \beta} \right)^{1/3}, \tag{22}$$

and

$$\frac{p_v - p}{L^2} = \frac{\left[1 + (3\Lambda^2 - 1)\,(R/\kappa_0)^3/2\right]}{\left[1 + (R/\kappa_0)^3\right]} \left[u^2 R \frac{\mathrm{d}^2 R}{\mathrm{d}x^2} + u R \frac{\mathrm{d}u}{\mathrm{d}x} \frac{\mathrm{d}R}{\mathrm{d}x} \right]$$

$$+\frac{3}{2}\,\frac{\left[1+2(2A^2-1)\,(R/\kappa_0)^3+A^2(R/\kappa_0)^6\right]}{\left[1+(R/\kappa_0)^3\right]^2}\,u^2\left(\frac{\mathrm{d}R}{\mathrm{d}x}\right)^2$$

$$+\frac{S_0}{L^2\,R}+\frac{4}{L^2\,(Re)}\,\frac{u}{R}\,\frac{\mathrm{d}R}{\mathrm{d}x}-\frac{p_{g0}}{L^2\,R^{3k}}\left[1-\frac{(\gamma-1)}{5\gamma}\,\frac{L}{\alpha}\,\frac{u}{R^2}\,\frac{\mathrm{d}R}{\mathrm{d}x}\,\delta_{k1}\right]. \quad (23)$$

In equations (19)–(23), δ_{k1} is the Kroneckar delta, L is the ratio of micro to macro scale given by

$$L=\frac{R_0'}{H_0'}, \quad (24)$$

κ_0 is given by

$$\kappa_0=\left(\frac{1-\beta_0}{\beta_0}\right)^{1/3}, \quad (25)$$

u_0 is the non-dimensional inlet velocity ($u_0=u_0'/\sqrt{p_0'/\rho_\ell'}$ with u_0' denoting the actual inlet velocity), Re and Re_ℓ are Reynolds numbers conveniently defined by

$$Re=\frac{H_0'\sqrt{p_0'/\rho_\ell'}}{\nu_D'}, \qquad Re_\ell=\frac{\rho_\ell'\,H_0'\sqrt{p_0'/\rho_\ell'}}{\mu_\ell'}, \quad (26)$$

φ is defined by

$$\varphi=\frac{H_0'\,\mathscr{P}'}{2\,A'}, \quad (27)$$

C_w is the wall friction coefficient, S_0 is the non-dimensional surface tension coefficient defined by

$$S_0=\frac{2\,S'}{p_0'\,R_0'}, \quad (28)$$

and α is the normalized thermal diffusivity of the gas defined by

$$\alpha=\frac{\alpha'}{\sqrt{p_0'/\rho_\ell'}\,R_0'}. \quad (29)$$

The normalized initial vapour pressure p_{g0} in (23) is fixed by the mechanical equilibrium condition at the nozzle inlet as

$$p_{g0}=1+S_0-p_v. \quad (30)$$

The normalized model equations (19)–(23) provide a coupled system of equations for the flow variables p, ρ, u, β and R provided that the normalized cross-sectional area A (nozzle shape) and p_v (usually taken as a constant by assuming isothermal conditions) are given.

3. The speed of sound and preliminary results

In this section, we consider the sonic speed of cavitating nozzle flows in the homogeneous flow model and discuss some general results underlying the model equations of the previous section. For this reason, we assume that the mixture density in the model under consideration is of the form of equation (1). When isothermal behaviour is assumed, the calculation of the sonic speed becomes straightforward (e.g. see van Wijngaarden 1972). From the definition of the speed of sound

$$\frac{1}{c'^2}=\frac{\mathrm{d}\rho'}{\mathrm{d}p'} \quad (31)$$

for isothermal flow, it follows by direct differentiation from (1) that

$$\frac{1}{c'^2} = \frac{(1-\beta)}{c_\ell'^2} - \rho_\ell' \frac{\mathrm{d}\beta}{\mathrm{d}p'}, \tag{32}$$

where

$$c_\ell'^2 = \frac{\mathrm{d}p'}{\mathrm{d}\rho_\ell'}, \tag{33}$$

with subscript ℓ denoting the liquid phase. By normalizing this sound speed in the same way as the normalization for the velocity and by writing $\mathrm{d}\beta/\mathrm{d}p' = (\mathrm{d}\beta/dx')/(\mathrm{d}p'/\mathrm{d}x')$, equation (32) takes the normalized form

$$\frac{1}{c^2} = \frac{(1-\beta)}{c_\ell^2} - \frac{\mathrm{d}\beta/\mathrm{d}x}{\mathrm{d}p/\mathrm{d}x}. \tag{34}$$

For convenience, let us define ω by

$$\omega = \frac{\lambda_0}{A}. \tag{35}$$

By solving from (19) and (20) for β and differentiating with respect to x, we can relate the derivative $\mathrm{d}\beta/\mathrm{d}x$ to $\mathrm{d}u/\mathrm{d}x$ and $\mathrm{d}\omega/\mathrm{d}x$ as

$$\frac{\mathrm{d}\beta}{\mathrm{d}x} = \frac{\omega}{u^2}\left(\frac{\mathrm{d}u}{\mathrm{d}x} - \frac{u}{\omega}\frac{\mathrm{d}\omega}{\mathrm{d}x}\right). \tag{36}$$

By substituting from (21) for $\mathrm{d}p/\mathrm{d}x$ and from (36) for $\mathrm{d}\beta/\mathrm{d}x$ into (34), we obtain

$$\frac{1}{c^2} = \frac{(1-\beta)}{c_\ell^2} + \frac{1}{u^2}\frac{\mathrm{d}u/\mathrm{d}x - (u/\omega)\mathrm{d}\omega/\mathrm{d}x}{\mathrm{d}u/\mathrm{d}x + \varphi u C_w - 4\mathrm{d}^2u/\mathrm{d}x^2/[3(Re_\ell)\omega]}. \tag{37}$$

Equation (37) yields an expression for the local speed of sound in the quasi-one-dimensional cavitating nozzle flow for the two-phase homogeneous flow model employed in the isothermal approximation. In particular, (37) at the throat ($\mathrm{d}\omega/\mathrm{d}x = 0$) reduces to

$$\frac{1}{c^{*2}} = \frac{(1-\beta^*)}{c_\ell^2} + \frac{1}{u^{*2}(1+\epsilon^*)}, \tag{38}$$

where

$$\epsilon^* = \frac{\varphi^* u^* C_w^* - 4(\mathrm{d}^2u/\mathrm{d}x^2)^*/[3(Re_\ell)\omega^*]}{(\mathrm{d}u/\mathrm{d}x)^*}, \tag{39}$$

provided that $(\mathrm{d}u/\mathrm{d}x)^* \neq 0$. In (38), c_ℓ is taken as a constant for isothermal flow and superscript * refers to the throat conditions. In the case where frictional effects can be neglected, which holds for most practical situations, equation (38) with $(\mathrm{d}u/\mathrm{d}x)^* \neq 0$ ($\epsilon^* \ll 1$), reduces to the inviscid flow result

$$\frac{1}{c^{*2}} = \frac{(1-\beta^*)}{c_\ell^2} + \frac{1}{u^{*2}}, \tag{40}$$

resulting in the flow speed exceeding the speed of sound at the throat ($u^* > c^*$). In the incompressible liquid limit, we obtain $u^* = c^*$, which was deduced by van Wijngaarden (1972). On the other hand, when $(\mathrm{d}u/\mathrm{d}x)^* = 0$, equation (37) for the speed of sound at the throat becomes

$$c^* = \frac{c_\ell}{\sqrt{1-\beta^*}}, \tag{41}$$

which for a dilute mixture becomes almost indistinguishable from its single-phase liquid flow value. The above expressions for the speed of sound were obtained by assuming a homogeneous two-phase flow model where the relative motion between the phases is neglected. It is well known that the speed of sound in two-phase mixtures is very much affected by the relative motion between the phases (e.g. see Noordzij & van Wijngaarden 1974). For cavitating flows, homogeneous flows in which the relative motion can be neglected require that the condition $R'/H_0' \ll 1$ be satisfied (e.g. see Brennen 1995 p. 152). For cavitating nozzle flows investigated here, this condition can be shown to hold for all solutions of the model equations except for those which lead to flow instabilities such as flashing flow solutions. Therefore, the above deductions for the speed of sound, which neglect the relative motion between the phases, are reasonable for all stable solutions.

Having discussed the speed of sound for quasi-one-dimensional cavitating nozzle flow in the isothermal approximation, we now deduce some general results, mainly from the equations of motion, which will be useful in interpreting the results from numerical simulations. In most practical cases, frictional effects can be neglected in the equations of motion. Consequently, (19) and (21) result in

$$\frac{\mathrm{d}}{\mathrm{d}x}\left(p + \tfrac{1}{2}u^2\right) = \beta u \frac{\mathrm{d}u}{\mathrm{d}x}. \tag{42}$$

The integration of (42) yields the generalized Bernoulli equation

$$p + \tfrac{1}{2}u^2 = 1 + \tfrac{1}{2}u_0^2 + \int_{u_0}^{u} \beta u \mathrm{d}u. \tag{43}$$

For incompressible flow with constant normalized density $1-\beta_0$, equation (43) reduces to the classical Bernoulli equation

$$\left[p + (1-\beta_0)\tfrac{1}{2}u^2\right]_{inc} = 1 + (1-\beta_0)\tfrac{1}{2}u_0^2 = \Lambda_0 \tag{44}$$

where subscript *inc* denotes incompressible flow. The generalized Bernoulli equation (43) together with (44) can then be written as

$$\left(p + \tfrac{1}{2}u^2\right) - \left(p + \tfrac{1}{2}u^2\right)_{inc} = \beta_0\left(\tfrac{1}{2}u_0^2 - \tfrac{1}{2}u_{inc}^2\right) + \int_{u_0}^{u} \beta u \mathrm{d}u. \tag{45}$$

In particular, in the initial growth region of the converging section of the nozzle where $\beta > \beta_0$, we have from (45)

$$\left(p + \tfrac{1}{2}u^2\right) - \left(p + \tfrac{1}{2}u^2\right)_{inc} > \beta_0\left(\tfrac{1}{2}u^2 - \tfrac{1}{2}u_{inc}^2\right) > 0, \tag{46}$$

since $u = \omega/(1-\beta) > u_{inc} = \omega/(1-\beta_0)$. Thus, in the converging section of the nozzle, we have the remarkable result

$$\left(p + \tfrac{1}{2}u^2\right) > \left(p + \tfrac{1}{2}u^2\right)_{inc}. \tag{47}$$

On the other hand, it also follows from (45) that

$$\left(p + \tfrac{1}{2}u^2\right) - \left(p + \tfrac{1}{2}u^2\right)_{inc} < \beta_0\left(\tfrac{1}{2}u_0^2 - \tfrac{1}{2}u_{inc}^2\right) + \beta\left(\tfrac{1}{2}u^2 - \tfrac{1}{2}u_0^2\right) \tag{48}$$

in the converging section of the nozzle, from which we deduce

$$p - p_{inc} < \tfrac{1}{2}\beta u^2 - \beta_0 \tfrac{1}{2}u_{inc}^2 - \left(\tfrac{1}{2}u^2 - \tfrac{1}{2}u_{inc}^2\right). \tag{49}$$

It follows by definition of u and u_{inc} that

$$\tfrac{1}{2}(u_{inc}^2 - u^2) = -(\beta - \beta_0)\,\omega^2 + O(\beta^2). \tag{50}$$

Substitution into (49) yields the result

$$p - p_{inc} < -\tfrac{1}{2}(\beta - \beta_0)\omega^2 + O(\beta^2). \tag{51}$$

Since, for a stable solution, $\omega \gg \beta$ and $\beta_0 < \beta \ll 1$ in the converging section, the term $O(\beta^2)$ can be neglected with respect to the first term of the right-hand side of inequality (51). Thus, for a stable solution, we have

$$p < p_{inc} \tag{52}$$

in the converging section of the nozzle. Inequalities (47) and (52) should hold in the converging section of the nozzle for any stable solution of the model equations.

4. The dynamical system and initial-value problem for the flow speed

We now return to the normalized model equations (19)–(23). We first note that different solutions of these model equations may emerge, depending on whether the problem is treated as an initial-value problem (IVP) by specifying only the initial conditions at the nozzle inlet or it is treated as an initial/boundary-value problem by specifying some additional condition such as the nozzle exit pressure (in the latter case the flow can be choked and shock waves may occur). In this investigation, we will restrict our discussion to an IVP of equations (19)–(23). It has already been demonstrated by Wang & Brennen (1997, 1998) and by Delale & Schnerr (1998) that the solution for the IVP of equations (19)–(23) for $\Lambda = 1$ may lead to flow instabilities such as flashing flow solutions. Here, we would like to demonstrate this instability on mathematical grounds and show how bubble/bubble interactions and/or various damping mechanisms can ramify the solution. To achieve this, we wish to uncouple equations (19)–(23) arriving at a single ordinary differential equation for a given nozzle configuration. For this reason, we note that the cavitating flow field will, most likely, be turbulent; therefore, the wall friction coefficient C_w should be calculated based on turbulent flow correlations. For single-phase turbulent correlations, the wall friction coefficient C_w can be written as a function of a conveniently defined flow Reynolds number Re_f and a relative roughness parameter ε as

$$C_w = C_w(Re_f, \varepsilon), \tag{53}$$

which, in turn, can be considered as a function of u and x. For cavitating flows, this relation can be very complicated and may depend on additional factors. With (53), it is indeed possible to reduce the complete system of (19)–(23) to a single third-order ordinary differential equation for the flow speed u. This is achieved as follows. From (19) and (20), we obtain

$$\beta = 1 - \frac{\omega}{u} \tag{54}$$

where ω is given by (35). Substitution from (54) into (22) yields

$$R = \kappa_0 \left(\frac{u}{\omega} - 1\right)^{1/3}. \tag{55}$$

By differentiating (55) twice with respect to x, and by substituting for $\mathrm{d}R/\mathrm{d}x$ and $\mathrm{d}^2R/\mathrm{d}x^2$ into the modified Rayleigh–Plesset equation (23), we arrive at the pressure–

velocity relation

$$p_v - p = A_1(u,x)\frac{\mathrm{d}^2u}{\mathrm{d}x^2} + B_1(u,x)\left(\frac{\mathrm{d}u}{\mathrm{d}x}\right)^2 + C_1(u,x)\frac{\mathrm{d}u}{\mathrm{d}x} + D_1(u,x), \tag{56}$$

where the coefficients $A_1(u,x)$, $B_1(u,x)$, $C_1(u,x)$ and $D_1(u,x)$ are given in Appendix A. Now by differentiating (56) with respect to x, and by substituting for $\mathrm{d}p/\mathrm{d}x$ together with the relation $\rho u = \omega$ into the momentum equation (21), we obtain the aforementioned third-order ordinary differential equation for the flow speed u of quasi-one-dimensional cavitating nozzle flows as

$$A(u,x)\frac{\mathrm{d}^3u}{\mathrm{d}x^3} + \left[B(u,x)\frac{\mathrm{d}u}{\mathrm{d}x} + C(u,x)\right]\frac{\mathrm{d}^2u}{\mathrm{d}x^2} + D(u,x)\left(\frac{\mathrm{d}u}{\mathrm{d}x}\right)^3 + E(u,x)\left(\frac{\mathrm{d}u}{\mathrm{d}x}\right)^2 + F(u,x)\frac{\mathrm{d}u}{\mathrm{d}x} + G(u,x) = 0, \tag{57}$$

where the coefficients $A(u,x)$, $B(u,x)$, $C(u,x)$, $D(u,x)$, $E(u,x)$, $F(u,x)$ and $G(u,x)$ are explicitly given in Appendix B. Equation (57) together with u_0, $(\mathrm{d}u/\mathrm{d}x)_0$ and $(\mathrm{d}^2u/\mathrm{d}x^2)_0$, where the subscript 0 refers to nozzle inlet-values, constitutes an initial-value problem for the flow speed u provided that the nozzle shape is given and that the parameters entering the coefficients given in Appendix B are related to the specified nozzle inlet conditions. In particular, $(\mathrm{d}u/\mathrm{d}x)_0$ and $(\mathrm{d}^2u/\mathrm{d}x^2)_0$ can be related to the nozzle inlet area and the inlet flow speed u_0 by

$$\left(\frac{\mathrm{d}u}{\mathrm{d}x}\right)_0 = u_0\left(\frac{1}{\omega}\frac{\mathrm{d}\omega}{\mathrm{d}x}\right)_0, \tag{58}$$

$$\left(\frac{\mathrm{d}^2u}{\mathrm{d}x^2}\right)_0 = u_0\left(\frac{1}{\omega}\frac{\mathrm{d}^2\omega}{\mathrm{d}x^2}\right)_0. \tag{59}$$

Equations (58) and (59) are equivalent to the inlet conditions $(\mathrm{d}R/\mathrm{d}x)_0 = 0$ and $(\mathrm{d}^2R/\mathrm{d}x^2)_0 = 0$. The latter condition can be obtained by considering the modified Rayleigh–Plesset equation (23) at the nozzle inlet together with the inlet mechanical equilibrium condition

$$(p_v)_0 = 1 + S_0 - p_{g0}. \tag{60}$$

The initial-value problem for (57) can be solved numerically (e.g. by the Runge–Kutta method); however, close examination of the coefficients $A(u,x)$, $B(u,x),\ldots$ given in Appendix B suggests a highly stiff nonlinear system with a singularity at $u = \omega$. For this reason, it is convenient to use the scaled variables ϕ, ψ and ζ defined by

$$\phi = \kappa_0^3(u - \omega), \tag{61}$$

$$\psi = \kappa_0^3\left(\frac{\mathrm{d}u}{\mathrm{d}x} - \frac{\mathrm{d}\omega}{\mathrm{d}x}\right) \tag{62}$$

and

$$\zeta = \kappa_0^3\left(\frac{\mathrm{d}^2u}{\mathrm{d}x^2} - \frac{\mathrm{d}^2\omega}{\mathrm{d}x^2}\right). \tag{63}$$

Now (57), after cumbersome manipulations, yields the dynamical system

$$\frac{\mathrm{d}\phi}{\mathrm{d}x} = \psi, \tag{64}$$

$$\frac{\mathrm{d}\psi}{\mathrm{d}x} = \zeta \tag{65}$$

and

$$\frac{\mathrm{d}\zeta}{\mathrm{d}x} = f(\phi, \psi, \zeta, x), \tag{66}$$

where

$$\begin{aligned}
f(\phi, \psi, \zeta, x) = {} & \frac{\phi}{\omega}\frac{d^3\omega}{dx^3} \\
& + \left[\frac{1}{3\phi}\left(\frac{\kappa_0^3\omega}{\phi+\kappa_0^3\omega}\right)^2\left\{\left[4-(18\Lambda^2-2)\frac{\phi}{\kappa_0^3\omega}-(27\Lambda^2-7)\left(\frac{\phi}{\kappa_0^3\omega}\right)^2\right]\zeta\right.\right. \\
& \left.\left.+\frac{\phi}{\omega}\left[8+4(9\Lambda^2+1)\frac{\phi}{\kappa_0^3\omega}+(45\Lambda^2-13)\left(\frac{\phi}{\kappa_0^3\omega}\right)^2\right]\frac{\mathrm{d}^2\omega}{\mathrm{d}x^2}\right\}\left(\psi-\frac{\phi}{\omega}\frac{\mathrm{d}\omega}{\mathrm{d}x}\right)\right. \\
& -\frac{8}{L^2\,(Re)\,\omega^{1/3}\phi^{2/3}}\left(\frac{\kappa_0^3\omega}{\phi+\kappa_0^3\omega}\right)^2\left\{\left[1+\left(1+\frac{Re}{Re_\ell}\right)\frac{\phi}{\kappa_0^3\omega}\right]\zeta\right. \\
& \left.+\frac{\phi}{\omega}\left[\frac{Re}{Re_\ell}-1-\frac{\phi}{\kappa_0^3\,\omega}\right]\frac{\mathrm{d}^2\omega}{\mathrm{d}x^2}\right\} \\
& -\frac{2(\gamma-1)p_{g0}\omega\delta_{k1}}{5\gamma L\alpha\phi^2}\left(\frac{\kappa_0^3\omega}{\phi+\kappa_0^3\omega}\right)\left(\zeta-\frac{\phi}{\omega}\frac{\mathrm{d}^2\omega}{\mathrm{d}x^2}\right) \\
& +2\left(\frac{\kappa_0^3\omega}{\phi+\kappa_0^3\omega}\right)^2\left[\frac{S_0}{L^2\,\omega\phi}-\frac{3kp_{g0}}{L^2\omega^{4/3-k}\phi^{k+2/3}}\right]\left(\psi-\frac{\phi}{\omega}\frac{\mathrm{d}\omega}{\mathrm{d}x}\right) \\
& +\frac{6\phi^{1/3}}{L^2\omega^{1/3}}\left(\frac{\kappa_0^3\omega}{\phi+\kappa_0^3\omega}\right)^2\left(\frac{\psi}{\kappa_0^3}+\frac{\mathrm{d}\omega}{\mathrm{d}x}+\frac{\mathrm{d}p_v/\mathrm{d}x+\varphi u\omega C_w}{\omega}\right) \\
& +\frac{8}{L^2\,(Re)\omega^{1/3}\phi^{5/3}}\left(\frac{\kappa_0^3\omega}{\phi+\kappa_0^3\omega}\right)^2\left(\psi-\frac{\phi}{\omega}\frac{\mathrm{d}\omega}{\mathrm{d}x}\right)\left(\psi+\frac{\phi^2}{\kappa_0^3\omega^2}\frac{\mathrm{d}\omega}{\mathrm{d}x}\right) \\
& +\frac{2(\gamma-1)p_{g0}\omega\delta_{k1}}{15\gamma L\alpha\phi^3}\left(\frac{\kappa_0^3\omega}{\phi+\kappa_0^3\omega}\right)^2\left[\left(1+4\frac{\phi}{\kappa_0^3\omega}\right)\psi-\frac{\phi}{\omega}\left(4+\frac{\phi}{\kappa_0^3\omega}\right)\frac{\mathrm{d}\omega}{\mathrm{d}x}\right] \\
& -\frac{1}{9\phi^2}\left(\psi-\frac{\phi}{\omega}\frac{\mathrm{d}\omega}{\mathrm{d}x}\right)\left\{\left[4-6(\Lambda^2-1)\frac{\phi}{\phi+\kappa_0^3\omega}\right]\left(\psi-\frac{\phi}{\omega}\frac{\mathrm{d}\omega}{\mathrm{d}x}\right)^2\right. \\
& -6\frac{\phi}{\omega}\left(\frac{\kappa_0^3\omega}{\phi+\kappa_0^3\omega}\right)\left(\psi-\frac{\phi}{\omega}\frac{\mathrm{d}\omega}{\mathrm{d}x}\right)\left[2\frac{\psi}{\kappa_0^3}-2\left(1+2\frac{\phi}{\kappa_0^3\omega}\right)\frac{\mathrm{d}\omega}{\mathrm{d}x}\right. \\
& \left.-3(\Lambda^2-1)\frac{\phi}{\phi+\kappa_0^3\omega}\left\{\frac{\psi}{\kappa_0^3}-\left(3+4\frac{\phi}{\kappa_0^3\,\omega}\right)\frac{\mathrm{d}\omega}{\mathrm{d}x}\right\}\right] \\
& +\frac{9\phi^2}{\omega^2}\left[2\left(\frac{\kappa_0^3\omega}{\phi+\kappa_0^3\omega}\right)^2\left(\frac{\psi}{\kappa_0^3}+\frac{\mathrm{d}\omega}{\mathrm{d}x}\right)^2-12\left(\frac{\kappa_0^3\omega}{\phi+\kappa_0^3\omega}\right)\left(\frac{\psi}{\kappa_0^3}+\frac{\mathrm{d}\omega}{\mathrm{d}x}\right)\frac{\mathrm{d}\omega}{\mathrm{d}x}\right. \\
& \left.\left.\left.+12\left(\frac{\mathrm{d}\omega}{\mathrm{d}x}\right)^2-3(\Lambda^2-1)\frac{\phi\kappa_0^3\omega}{(\phi+\kappa_0^3\,\omega)^2}\left\{\frac{\psi}{\kappa_0^3}-\left(1+2\frac{\phi}{\kappa_0^3\,\omega}\right)\frac{\mathrm{d}\omega}{\mathrm{d}x}\right\}\right]\right\}\right] \\
& \times\left[2+3(\Lambda^2-1)\frac{\phi}{\phi+\kappa_0^3\omega}\right]^{-1}.
\end{aligned} \tag{67}$$

The dynamical system of equations (64)–(67) with initial values

$$\phi_0 = \omega_0 = \lambda_0, \tag{68}$$

$$\psi_0 = \left(\frac{\mathrm{d}\omega}{\mathrm{d}x}\right)_0 = -\lambda_0 \left(\frac{\mathrm{d}A}{\mathrm{d}x}\right)_0 \tag{69}$$

and

$$\zeta_0 = \left(\frac{\mathrm{d}^2\omega}{\mathrm{d}x^2}\right)_0 = \lambda_0 \left[2\left(\frac{\mathrm{d}A}{\mathrm{d}x}\right)_0^2 - \left(\frac{\mathrm{d}^2A}{\mathrm{d}x^2}\right)_0\right] \tag{70}$$

constitutes an initial-value problem for the scaled variables ϕ, ψ and ζ provided that the parameters Λ, Re, β_0, S_0, the ratio of Re/Re_ℓ together with the constant k and the distributions of the normalized reciprocal area $\omega(x)$, the normalized partial vapour pressure $p_v(x)$ and a model for the wall friction coefficient $C_w(u, x)$ are specified.

The dynamical system given above by (64)–(67) is a nonlinear non-autonomous system in three variables. It is, therefore, very complicated for general analysis. It may not even satisfy a local Lipschitz condition since it contains many parameters and distributions. Consequently, instabilities may occur and bifurcation of solutions may result for some values of the parameters and specified distributions, as has already been demonstrated by Wang & Brennen (1997, 1998) numerically.

5. The hydrodynamic field

The hydrodynamic variables can be related to the scaled variables ϕ, ψ and ζ; therefore, the solution of the initial-value problem for the dynamical system of (64)–(67) together with the initial values (68)–(70) completely determines the hydrodynamic field. In particular, the normalized velocity field and its derivatives can be evaluated directly from

$$u = \frac{\phi}{\kappa_0^3} + \omega, \tag{71}$$

$$\frac{\mathrm{d}u}{\mathrm{d}x} = \frac{\psi}{\kappa_0^3} + \frac{\mathrm{d}\omega}{\mathrm{d}x} \tag{72}$$

and

$$\frac{\mathrm{d}^2u}{\mathrm{d}x^2} = \frac{\zeta}{\kappa_0^3} + \frac{\mathrm{d}^2\omega}{\mathrm{d}x^2}. \tag{73}$$

The void fraction β (consequently the normalized mixture density ρ) and the normalized radius R can then be found by directly substituting for u from (71) into (54) and (55), respectively, to arrive at

$$\beta = 1 - \rho = \frac{\phi}{\phi + \kappa_0^3 \omega} \tag{74}$$

and

$$R = \left(\frac{\phi}{\omega}\right)^{1/3}. \tag{75}$$

The pressure field follows by substituting from (71)–(73) for u and its derivatives into

the pressure–velocity relation (56) which yields

$$
\begin{aligned}
p_v - p = {} & \frac{L^2\omega^{4/3}}{6\phi^{1/3}}\left(1+\frac{\phi}{\kappa_0^3\omega}\right)^2\left[2+3(\Lambda^2-1)\frac{\phi}{\phi+\kappa_0^3\omega}\right]\left(\zeta-\frac{\phi}{\omega}\frac{\mathrm{d}^2\omega}{\mathrm{d}x^2}\right)\\
& -\frac{L^2\omega^{4/3}}{18\phi^{4/3}}\left(1+\frac{\phi}{\kappa_0^3\omega}\right)^2\left[1-6\Lambda^2\frac{\phi}{\phi+\kappa_0^3\omega}\right]\left(\psi-\frac{\phi}{\omega}\frac{\mathrm{d}\omega}{\mathrm{d}x}\right)^2\\
& -\frac{L^2\omega^{1/3}}{6\phi^{1/3}}\left(1+\frac{\phi}{\kappa_0^3\omega}\right)^2\left[2+3(\Lambda^2-1)\frac{\phi}{\phi+\kappa_0^3\omega}\right]\left(\psi-\frac{\phi}{\omega}\frac{\mathrm{d}\omega}{\mathrm{d}x}\right)\frac{\mathrm{d}\omega}{\mathrm{d}x}\\
& +\left(1+\frac{\phi}{\kappa_0^3\omega}\right)\left[\frac{4\omega}{3(Re)\phi}+\frac{(\gamma-1)p_{g0}L\omega^{7/3}\delta_{k1}}{15\gamma\alpha\phi^{7/3}}\right]\left(\psi-\frac{\phi}{\omega}\frac{\mathrm{d}\omega}{\mathrm{d}x}\right)\\
& +S_0\left(\frac{\omega}{\phi}\right)^{1/3}-p_{g0}\left(\frac{\omega}{\phi}\right)^k. \qquad (76)
\end{aligned}
$$

6. Results and discussion

In this section, we would like to determine the solution of the initial-value problem for the dynamical system given by (64)–(70) with smooth area variation. For this reason, we first relate the parameters u_0, Re, and S_0 to the conventionally used inlet cavitation number σ_0, Reynolds number Re_{R0} and Weber number We_{R0} by

$$\sigma_0 \equiv \frac{p_0' - p_v'}{(1/2)\rho_\ell' u_0'^2} = \frac{2(1-p_v)}{u_0^2}, \qquad (77)$$

$$Re_{R0} \equiv \frac{u_0' R_0'}{\nu_D'} = u_0 L(Re) \qquad (78)$$

and

$$We_{R0} \equiv \frac{u_0'^2 \rho_\ell' R_0'}{S'} = \frac{2}{S_0}u_0^2, \qquad (79)$$

where p_v is taken as a constant evaluated from the saturated vapour pressure corresponding to the isothermal temperature, and L is the ratio of the micro to macro scale given by (25). Therefore, for given σ_0, Re_{R0} and We_{R0}, the parameters u_0, Re and S_0 entering the dynamical system can be calculated from (77)–(79) as

$$u_0 = \left(\frac{2(1-p_v)}{\sigma_0}\right)^{1/2}, \qquad (80)$$

$$Re = \frac{(Re_{R0})}{L\left[2(1-p_v)/\sigma_0\right]^{1/2}} \qquad (81)$$

and

$$S_0 = \frac{4(1-p_v)}{\sigma_0(We_{R0})}. \qquad (82)$$

Now for given isothermal temperature T' of the liquid (for which the corresponding partial vapour pressure p_v' and the surface tension coefficient S' can be evaluated), inlet cavitation number σ_0, Reynolds number Re_{R0}, Weber number We_{R0}, ratio of micro to macro scale L (or initial radius R_0'), inlet void fraction β_0 (from which κ_0 is evaluated), ratio of $Re/Re_\ell = \nu_\ell'/\nu_D'$ and bubble/bubble interaction parameter Λ, the initial-value problem for the dynamical system (64)–(70) can be solved very accurately

employing a fourth-order Runge–Kutta method provided that the function φ defined by (27), the wall friction coefficient C_w and the reciprocal normalized area $\omega(x)$ are specified. For a quasi-one-dimensional nozzle, it can be easily shown that

$$\varphi = \frac{1}{A}. \tag{83}$$

The wall friction coefficient C_w can be evaluated by (53) for a smooth wall using the two-dimensional turbulent correlation, which was verified experimentally by Laufer (1950) (for details see Ward-Smith 1980),

$$\frac{1}{C_w^{1/2}} = 1.768 \ln \left[(Re_f) C_w^{1/2} \right] - 0.94, \tag{84}$$

where the flow Reynolds number Re_f is defined by

$$Re_f = \frac{2Q_f'}{\nu_\ell'} = 2uARe_\ell, \tag{85}$$

with Q_f' denoting the incompressible volumetric flow rate per unit width of the nozzle and with Re_ℓ given by (26). For the normalized area A, we use two nozzles: one used by Schulz (1995), and given by

$$\begin{aligned} A(x) = {} & 0.8 - 0.00254118\,x + 0.12238569\,x^2 - 0.26540443\,x^3 - 0.85375693\,x^4 \\ & -1.3807352\,x^5 - 1.3813923\,x^6 - 0.81149967\,x^7 - 0.25638892\,x^8 \\ & -0.033676342\,x^9 \quad \text{for} \quad x \leqslant 0 \end{aligned}$$

and

$$\begin{aligned} A(x) = {} & 0.8 - 0.00254118\,x + 0.12238569\,x^2 - 0.26540443\,x^3 + 0.46149\,x^4 \\ & -0.42670\,x^5 + 0.21927\,x^6 - 0.063639\,x^7 - 0.0097241\,x^8 \\ & -0.00060396\,x^9 \quad \text{for} \quad x \geqslant 0, \end{aligned} \tag{86}$$

where the origin of the x-axis is chosen at the nozzle throat (referred to as nozzle 1) and another one used by Wang & Brennen (1997, 1998), and given by

$$A(x) = \frac{1}{2} \left[3 + \cos \left(\frac{2\pi x}{500\,L} \right) \right]^{1/2} \quad \text{for} \quad 0 \leqslant \frac{x}{L} \leqslant 500$$

and

$$A(x) = 1 \quad \text{for} \quad \frac{x}{L} \geqslant 500, \tag{87}$$

where the origin of the x-axis is chosen at the nozzle inlet (referred to as nozzle 2). As can be seen clearly from figure 1, nozzle 2 seems to be more convenient for two-dimensional calculations and will be employed only to compare the results of this investigation with those of Wang & Brennen (1997, 1998) under the same specified conditions.

For both nozzles, a two-phase bubbly flow with bubbles containing water vapour and air in water at an isothermal temperature of 20°C, implying a constant partial vapour pressure $p_v' = 0.0234$ bar, a constant surface tension coefficient $S' = 7.1 \times 10^{-2}$ N m^{-1} and a constant water viscosity $\mu_\ell' = 10^{-3}$ kg m^{-1} s^{-1}, is considered. Under these conditions, we first find the solution of the initial-value problem of the dynamical system (64)–(70) for $\Lambda = 1$ and $Re = Re_\ell$, corresponding to the case where bubble/bubble interactions are neglected and where the only damping mechanism is

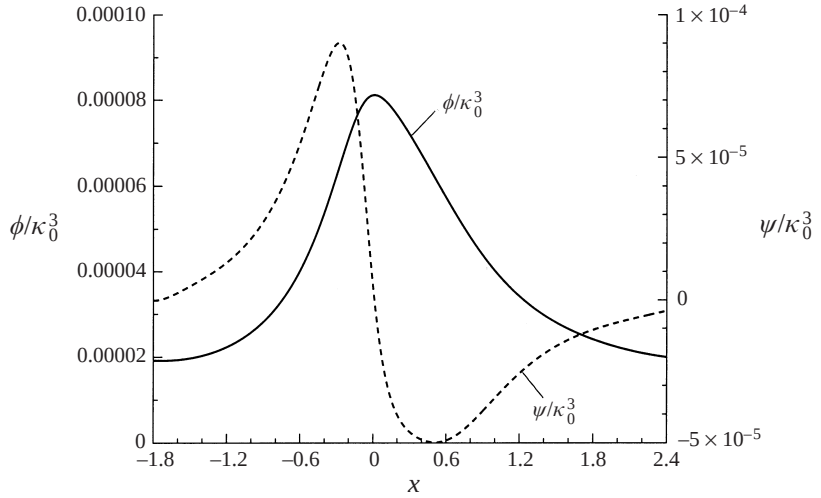

FIGURE 3. A stable solution of the dynamical system (64)–(70) with viscous damping only ($Re_\ell/Re = 1$) and without bubble/bubble interactions ($\Lambda = 1$) for the scaled variables ϕ and ψ for water vapour–air bubbles in water at an isothermal temperature of 20°C representing limited growth and collapse of bubbles along the axis of nozzle 1 with initial void fraction $\beta_0 = 10^{-5}$, initial cavitation number $\sigma_0 = 0.5$, Reynolds number $Re_{R0} = 50$, Weber number $We_{R0} = 7.04225$ and ratio of micro to macro scale $L = 5 \times 10^{-5}$ (corresponding to inlet flow speed $u_0' = 10$ m s^{-1} and initial radius $R_0' = 5$ μm).

viscous damping. For nozzle 1, with inlet height $H_0' = 0.1$ m, the initial cavitation number σ_0, the initial void fraction β_0 and the inlet flow speed u_0' are fixed at the values $\sigma_0 = 0.5$, $\beta_0 = 10^{-5}$ and $u_0' = 10$ m s^{-1} respectively. The initial radius R_0' is varied from 5 μm to 12 μm and the results are shown in figures 3–8. Figures 3–5 show a stable solution for $R_0' = 5$ μm (corresponding to $Re_{R0} = 50$, $We_{R0} = 7.04225$ and $L = 5 \times 10^{-5}$). Figure 3 exhibits the solution of the initial-value problem of the dynamical system (64)–(70) for ϕ and ψ. In this case, ϕ exhibits a maximum at the throat ($x = 0$) where ψ vanishes. The variations of the normalized radius R and of the pressure coefficient C_p, defined by

$$C_p = \frac{p' - p_0'}{0.5\rho_\ell' u_0'^2} = \frac{p-1}{0.5u_0^2}, \tag{88}$$

for this case are shown in figure 4. Here, the bubble grows to its maximum value (about 1.5 times its initial radius) at the throat. The pressure coefficient almost coincides with the incompressible single-phase pressure coefficient $(C_p)_{inc}$ although $C_p < (C_p)_{inc}$, as implied by (52) (in this case $C_p - (C_p)_{inc} = O(\beta) = O(10^{-5})$ to $O(10^{-4})$ numerically, which cannot be distinguished on the scale of figure 4). The corresponding variations of the void fraction β and the flow speed u are shown in figure 5. Figures 6–8 show a flashing flow solution for $R_0' = 12$ μm with the rest of the independent parameters held fixed. Figure 6 exhibits the ever increasing solution of the dynamical system for ϕ and ψ, whereas figure 7 shows the distributions of the normalized radius R and of the pressure coefficient C_p and its incompressible single-phase value $(C_p)_{inc}$. Figure 8 shows the corresponding distributions of the void fraction β and of the normalized flow speed u. In this case, the flow flashes before it reaches the throat. Once again, the distributions of C_p and $(C_p)_{inc}$ (with $C_p < (C_p)_{inc}$) almost coincide, except for

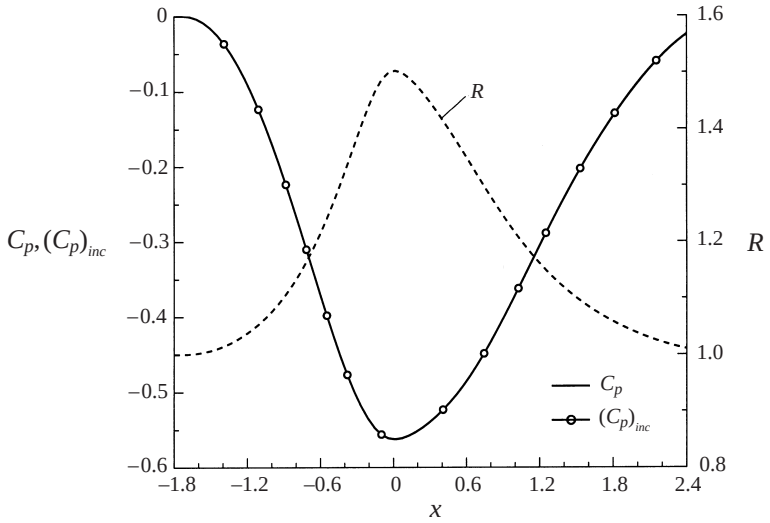

FIGURE 4. Distributions of the normalized radius R, the pressure coefficient C_p and its incompressible single-phase value $(C_p)_{inc}$ along the axis of nozzle 1 under the conditions stated in figure 3.

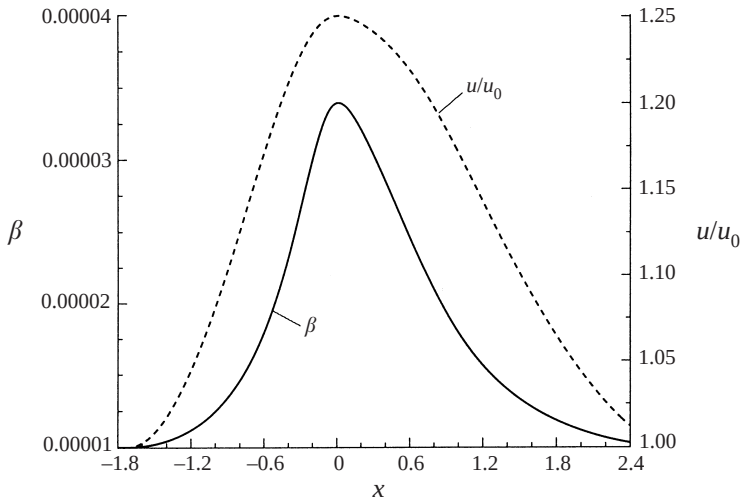

FIGURE 5. Distributions of the normalized flow speed u/u_0 and the void fraction β along the axis of nozzle 1 under the conditions stated in figure 3.

the very thin zone near the throat ($x = 0$) where enormous deviations build up. In summary, the flow field in nozzle 1 exhibits instabilities inherited from the nature of the dynamical system (64)–(70) as the initial radius is increased from $R_0' = 5$ μm to $R_0' = 12$ μm with a bifurcation at $R_0' = 10.2245 \pm 0.0005$ μm to a flashing flow solution when the rest of the parameters are held fixed. It is worthwhile to mention that no significant changes are observed in either of the stable or flashing solutions when wall shear effects are taken into account by (84). As reasoned in Appendix C,

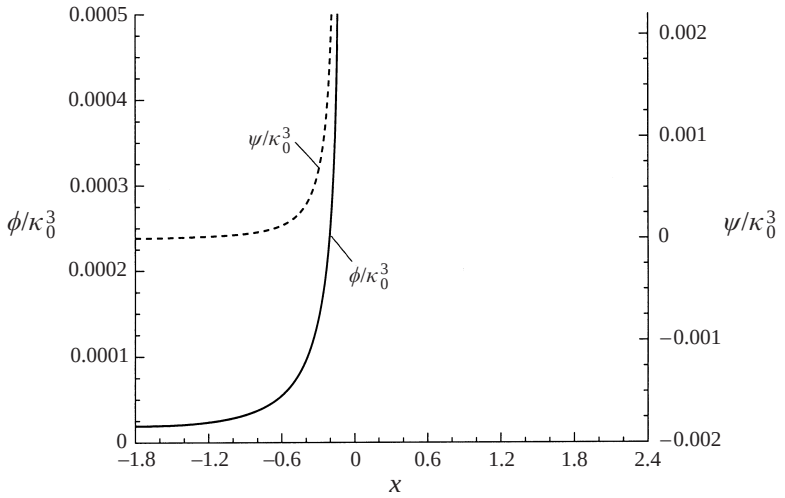

FIGURE 6. Flashing flow solution of the dynamical system (64)–(70) with viscous damping only ($Re_\ell/Re = 1$) and without bubble/bubble interactions ($\Lambda = 1$) for the scaled variables ϕ and ψ for water vapour–air bubbles in water at an isothermal temperature of 20°C along the axis of nozzle 1 with initial void fraction $\beta_0 = 10^{-5}$, initial cavitation number $\sigma_0 = 0.5$, Reynolds number $Re_{R0} = 120$, Weber number $We_{R0} = 16.90141$ and ratio of micro to macro scale $L = 1.2 \times 10^{-4}$ (corresponding to inlet flow speed $u_0' = 10$ m s^{-1} and initial radius $R_0' = 12$ μm).

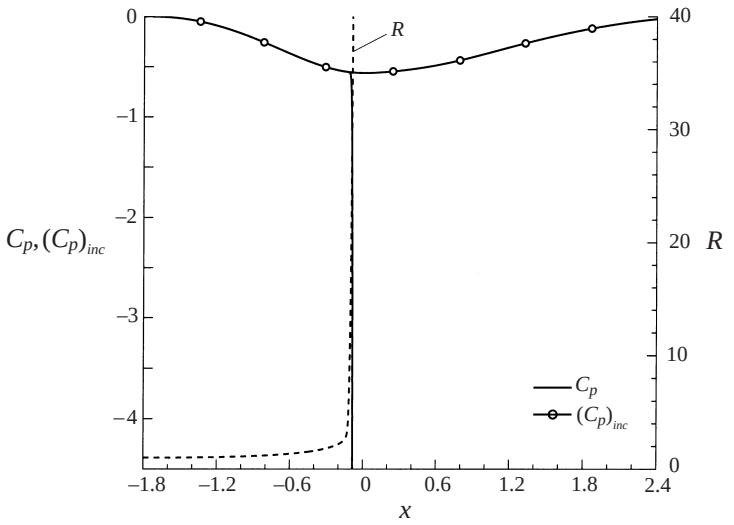

FIGURE 7. Flashing flow distributions of the normalized radius R, the pressure coefficient C_p and its incompressible single-phase value $(C_p)_{inc}$, along the axis of nozzle 1 under the conditions stated in figure 6.

the occurrence of this instability during the growth period of bubbles in cavitating nozzle flows is mainly due to the use of the classical Rayleigh–Plesset equation for bubble dynamics (equation (23) with $\Lambda = 1$ and $Re = Re_\ell$) and, as will be discussed later, it can be overcome by taking into account bubble/bubble interactions ($\Lambda \gg 1$).

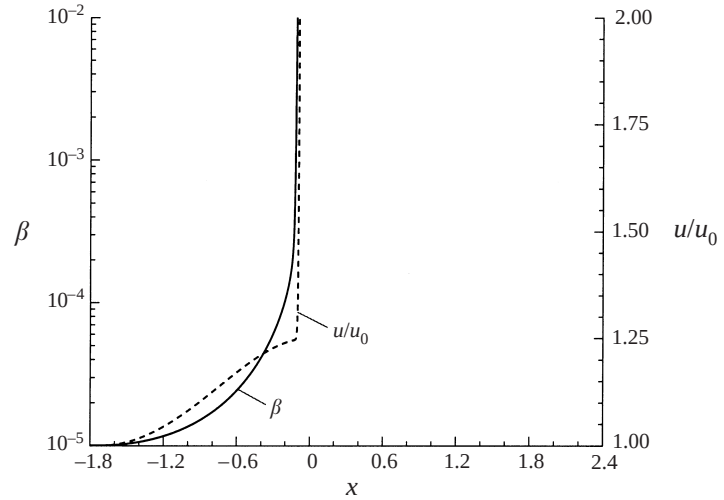

FIGURE 8. Flashing flow distributions of the normalized flow speed u/u_0 and the void fraction β along the axis of nozzle 1 under the conditions stated in figure 6.

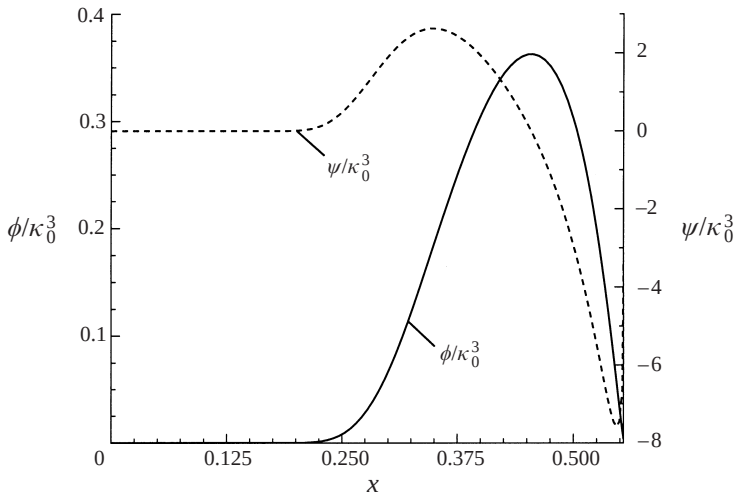

FIGURE 9. Flashing flow solution of the dynamical system (64)–(70) with viscous damping only ($Re_\ell/Re = 1$) and without bubble/bubble interactions ($\Lambda = 1$) for the scaled variables ϕ and ψ for water vapour-air bubbles in water at an isothermal temperature of 20°C with a single rebound structure along the axis of nozzle 2 with initial void fraction $\beta_0 = 6 \times 10^{-6}$, initial cavitation number $\sigma_0 = 0.8$, Reynolds number $Re_{R0} = 1000$, Weber number $We_{R0} = 137$ and ratio of micro to macro scale $L = 10^{-3}$ (corresponding to inlet flow speed $u_0' = 10$ m s^{-1} and initial radius $R_0' = 100$ μm).

A similar type of behaviour, i.e. bifurcation of the flow to a flashing solution, has already been found by Wang & Brennen (1997, 1998) for nozzle 2.

We now compare the solution for the initial-value problem of the system of equations (64)–(70) for $\Lambda = 1$ with the numerical results of Wang & Brennen (1997, 1998) in nozzle 2 under the same specified conditions. For this reason, we fix the initial

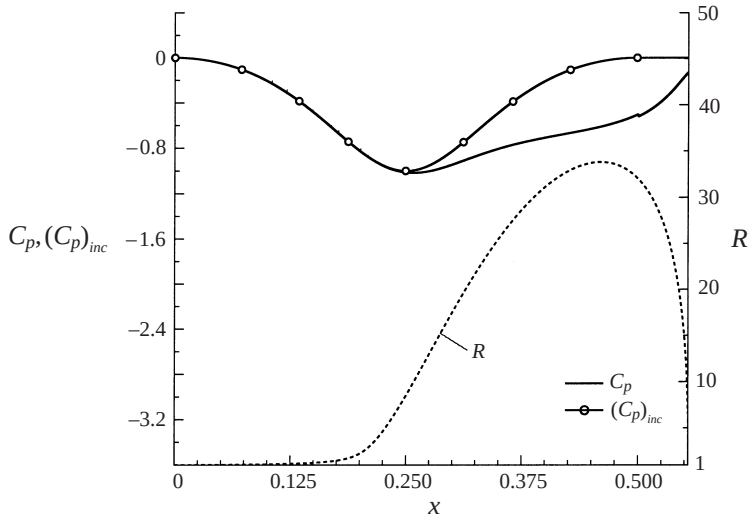

FIGURE 10. Flashing flow distributions of the normalized radius R, the pressure coefficient C_p and its incompressible single-phase value $(C_p)_{inc}$, along the axis of nozzle 2 under the conditions stated in figure 9.

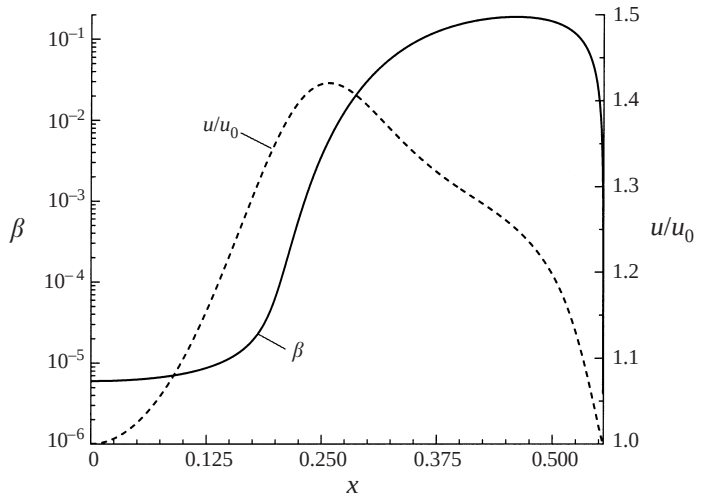

FIGURE 11. Flashing flow distributions of the normalized flow speed u/u_0 and the void fraction β along the axis of nozzle 2 under the conditions stated in figure 9.

cavitation number at $\sigma_0 = 0.8$, the Reynolds number at $Re_{R0} = 1000$, Weber number at $We_{R0} = 137$ and the ratio of micro to macro scale at $L = 10^{-3}$ (corresponding to the fixed initial flow speed $u_0' = 10$ m s^{-1}, fixed initial radius $R_0' = 100$ μm and fixed nozzle inlet height $H_0' = 0.1$ m) and vary the initial void fraction β_0 between 6.0×10^{-6} and 7.0×10^{-6} (in contrast to the numerical results given by Wang & Brennen (1997) where β_0 is varied between 2.0×10^{-6} and 2.9×10^{-6} for the same fixed values of the rest of the parameters). Typical results for the case with $\beta_0 = 6.0 \times 10^{-6}$ are plotted in figures 9–11. In all of these figures, the origin of the axis of nozzle 2 is chosen

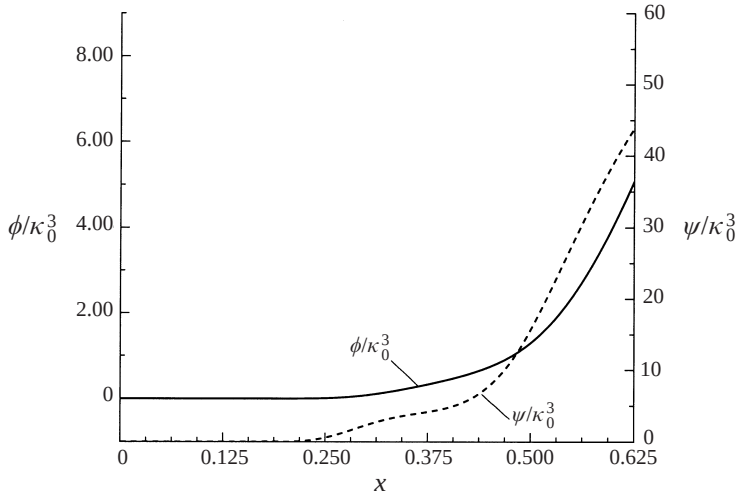

FIGURE 12. Flashing flow solution of the dynamical system (64)–(70) with viscous damping only ($Re_\ell/Re = 1$) and without bubble/bubble interactions ($\Lambda = 1$) for the scaled variables ϕ and ψ for water vapour–air bubbles in water at an isothermal temperature of 20°C with no rebound structure along the axis of nozzle 2 with initial void fraction $\beta_0 = 7 \times 10^{-6}$, initial cavitation number $\sigma_0 = 0.8$, Reynolds number $Re_{R0} = 1000$, Weber number $We_{R0} = 137$ and ratio of micro to macro scale $L = 10^{-3}$ (corresponding to inlet flow speed $u_0' = 10$ m s^{-1} and initial radius $R_0' = 100$ μm).

at $x = 0$ with the throat located at $x = 0.25$. Figure 9 shows the solution of the dynamical system (64)–(70) for ϕ and ψ. Contrary to the previously discussed stable solution in nozzle 1, ϕ does not exhibit a maximum at the throat ($x = 0.25$) in this case. The maximum is shifted to the diverging section of the nozzle downstream of the throat. The solution for ϕ then decreases (corresponding to the collapse of the bubble) and this decrease continues even in the constant area section ($x > 0.5$) with an almost abrupt change towards a flashing flow solution (which is not shown in the figure). Figure 10 shows the corresponding distributions for the normalized radius R and for the pressure coefficients C_p and $(C_p)_{inc}$. We observe that the bubble is still growing at the throat, exhibits a maximum in the diverging section and then collapses (after this rebound, the flow flashes which is not shown in the figure). The pressure coefficient C_p deviates considerably from its incompressible value $(C_p)_{inc}$ downstream of the throat and exhibits a real jump at $x = 0.5$ where the second- and higher-order derivatives of the area are discontinuous, as expected (the fact that the jumps in the derivatives of ω at some point leads to a jump in the pressure coefficient can be seen from (76)). This observation demonstrates the high level of precision achieved in the solution of the initial-value problem of the dynamical system (64)–(70). Figure 11 shows the corresponding distributions for the void fraction β and for the normalized flow speed u. For this case, wall shear effects, given by (84), can be neglected. Figures 12–14 show a different type of solution in nozzle 2 for $\beta_0 = 7.0 \times 10^{-6}$ with the rest of the parameters held fixed. Figure 12 shows a flashing flow solution (with no rebound structure) for ϕ and ψ, whereas figure 13 displays the corresponding distributions for the normalized radius R and for the pressure coefficients C_p and $(C_p)_{inc}$. Once again, notice the jump in C_p at $x = 0.5$ owing to the discontinuities in the derivatives of the normalized area. The flashing flow distributions for the void fraction β and for the normalized flow speed u in nozzle 2 are shown in figure 14. Wall shear effects,

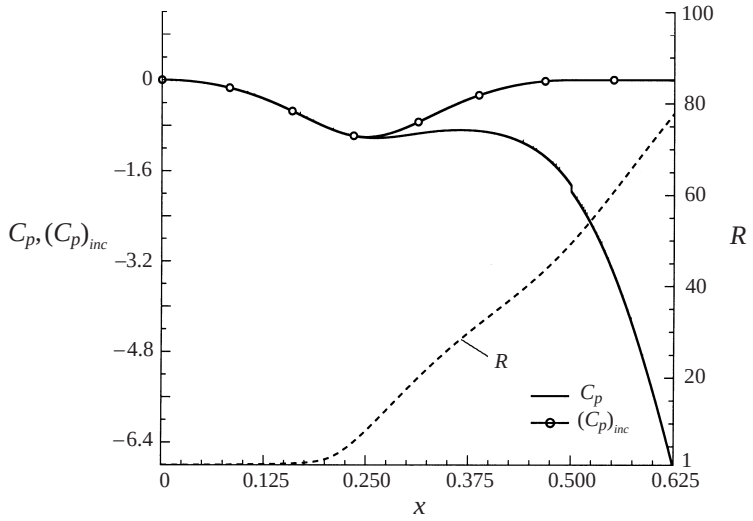

FIGURE 13. Flashing flow distributions, with no rebound structure, of the normalized radius R, the pressure coefficient C_p and its incompressible single-phase value $(C_p)_{inc}$, along the axis of nozzle 2 under the conditions stated in figure 12.

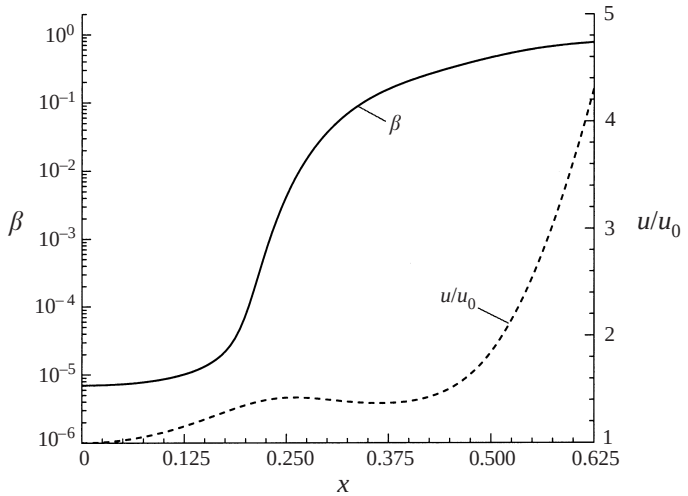

FIGURE 14. Flashing flow distributions, with no rebound structure, of the normalized flow speed u/u_0 and the void fraction β along the axis of nozzle 2 under the conditions stated in figure 12.

given by (84), also seem to be insignificant for this case. In summary, for the cases investigated, two types of flow patterns emerge for nozzle 2:

(i) A flashing flow solution with no rebound structure at $\beta_0 = 7.0 \times 10^{-6}$, and

(ii) a flashing flow structure with a single rebound (growth and collapse of the bubble) at $\beta_0 = 6.0 \times 10^{-6}$,

with the rest of the parameters held fixed at the values given above and in the figure captions. The bifurcation from one type of solution to the other occurs at

approximately $\beta_0 = 6.1785 \pm 0.0005 \times 10^{-6}$. In both cases, the flow flashes showing that there are no stable steady-state solutions for these cases in the model considered ($\Lambda = 1$ and $Re = Re_\ell$). A comparison of our results for nozzle 2 with those of Wang & Brennen (1997) under similar conditions (actually the same conditions except for the range of β_0) show similarities as well as differences. The main difference is that no stable solution can be found for the solution of the dynamical system (64)–(70) exhibited in figures 10–12 (the flow flashes after a rebound, i.e. growth and collapse of bubbles) in contrast to the quasi-statically stable ringing structure obtained in the constant area section ($x > 0.5$) by Wang & Brennen (1997). Although the growth and collapse structures of the first rebound look similar in both cases, our calculations show that the flow immediately flashes after the first rebound (unstable solution), whereas the rebound is repeated to form a ringing structure (stable solution) in the results of Wang & Brennen. The extremely high gradients in the flow variables after the first rebound seem to be responsible for this type of flashing solution, preventing the formation of a stable ringing structure in our calculations. The second difference is the quantitative difference in the bifurcation value of β_0 (the bifurcation reported by Wang & Brennen (1997) occurs at $\beta_0 = 2.862 \times 10^{-6}$ compared to our value at $\beta_0 = 6.1785 \pm 0.0005 \times 10^{-6}$) occurring between the two types of different structure in each case. The numerical error inherited from integration of coupled equations of flow and bubble dynamics for $\Lambda = 1$ may be the source of this second difference.

Wang & Brennen (1998) also considered the effect of damping mechanisms (liquid viscosity, thermal damping, acoustic radiation, etc.) by introducing a damping coefficient (in the same form as in (14)) into the Rayleigh–Plesset equation (a value of such a damping coefficient in the Rayleigh–Plesset equation that compares well with experiments for spherical clouds is recently given by Colonius *et al.* 1998). With such a damping coefficient, they reproduced the calculations by reducing the Reynolds number Re_{R0} from a value of 1000 to a value of 33 (corresponding to increasing the ratio Re_ℓ/Re from unity to 30) keeping the rest of the variables fixed for nozzle 2 and varying the void fraction between 2.5×10^{-6} and 3.1×10^{-6}. Their results showed the same structural considerations discussed above with some reduction in the maximum attainable bubble radii along the nozzle axis for the case of their quasi-statically stable flow with rebound structure downstream of the throat and with a shift to a value of $\beta_0 = 3.045$ for the bifurcation to a flashing flow. For comparison with our calculations we choose the same conditions for nozzle 2 as stated in the caption of figure 12, but now vary Re_{R0} between 10 and 1000 (this corresponds to varying Re_ℓ/Re, between 1 and 100). The results for the normalized bubble radius R and the pressure coefficient C_p are shown in figure 15. The effect of damping ($Re_\ell/Re \geqslant 1$) can clearly be seen from this figure. For the cases where Re_{R0} assumes the values 100 and 10, corresponding to Re_ℓ/Re equal to 10 and 100, respectively, the maximum radii are lowered with a shift of the collapse zones toward the throat. The pressure coefficients C_p show, respectively, a slight increase followed by an instability of ever decreasing solution for $Re_{R0} = 100$ in the constant area section downstream the throat, and an ever increasing value resulting from instabilities in the diverging section of the nozzle for $Re_{R0} = 10$ (the case $Re_{R0} = 1000$ corresponds to the solution with $Re_\ell/Re = 1$). These instabilities seem to arise from extremely high gradients of the flow variables either during collapse or rebound. Notice also that the instability leads to an ever increasing pressure coefficient C_p in the diverging section of nozzle 2, whereas it leads to decreasing pressure coefficients C_p in the constant area section of nozzle 2. Therefore, the damping mechanisms introduced into the Rayleigh–Plesset equation by a damping coefficient in the form of viscous dissipation, do not seem to overcome

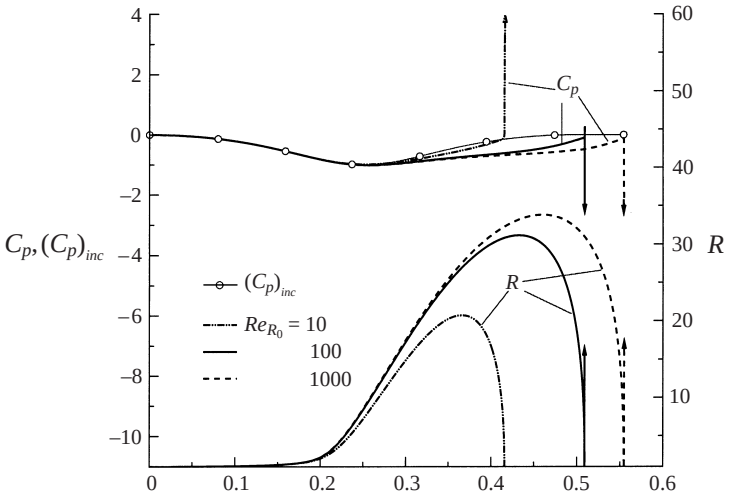

FIGURE 15. The effect of damping mechanisms by a damping coefficient on the distributions of the normalized radius R and the pressure coefficient C_p along the axis of nozzle 2 under the conditions stated in figure 9 and for Reynolds number Re_{R0} assuming values 10, 100 and 1000 (corresponding to Re_ℓ/Re, respectively, equal to 100, 10 and 1).

the instabilities observed for nozzle 2 in the model considered ($\Lambda = 1$). For the cases investigated, it is worthwhile to mention that the sensitivity of the flow with respect to instabilities seems to be greatest when the area variations are small. Consequently, the slenderness of the nozzle turns out to be an important parameter.

Having demonstrated the instabilities for the initial-value problem of the model equations (19)–(23) for $\Lambda = 1$ (the classical Rayleigh–Plesset equation coupled to the quasi-one-dimensional steady nozzle flow equations) in both nozzles, it is important to see the physical ramifications of these instabilities. In doing so, we will consider these ramifications for nozzle 1 alone since it fits more into the quasi-one-dimensional flow description (see figure 1). As was shown in nozzle 2, the use of a damping coefficient (in the form of viscous dissipation) alone in the Rayleigh–Plesset equation for damping mechanisms does not seem to overcome the instabilities. Therefore, we first try to study these ramifications by taking into account bubble/bubble interactions ($\Lambda \gg 1$) with viscous damping only ($k = 1$, $\alpha \to \infty$ and $Re_\ell/Re = 1$). In particular, we investigate the effect of bubble/bubble interactions on the flashing flow solution exhibited in figures 6–8 in nozzle 1 under the same conditions as specified in figure 6. Figures 16–18 demonstrate how the instability disappears for the value of the interaction parameter $\Lambda = 300$ leading to a stable cavitating flow solution with continuous growth of bubbles (continuous evaporation). If the interaction parameter Λ is further increased, a single rebound structure (evaporation followed by condensation) with collapsing bubbles at the nozzle exit is observed. Figures 19–21 show such a stable cavitating flow with collapsing bubbles at the nozzle exit. If the interaction parameter Λ is increased beyond a certain value, collapsing structure instabilities set in with ever decreasing radii of bubbles corresponding to the pressure coefficient C_p increasing without bound. Such an unstable solution is shown in figures 22–24 for $\Lambda = 400$. In summary, the flashing flow instability in nozzle 1 for $\Lambda = 1$ under the conditions specified in figure 6 can be overcome by taking into account bubble/bubble interactions in our model for the range of the interaction parameter $285 < \Lambda < 375$ resulting in stable steady cavitating nozzle flow solutions either with continuous growth of bubbles

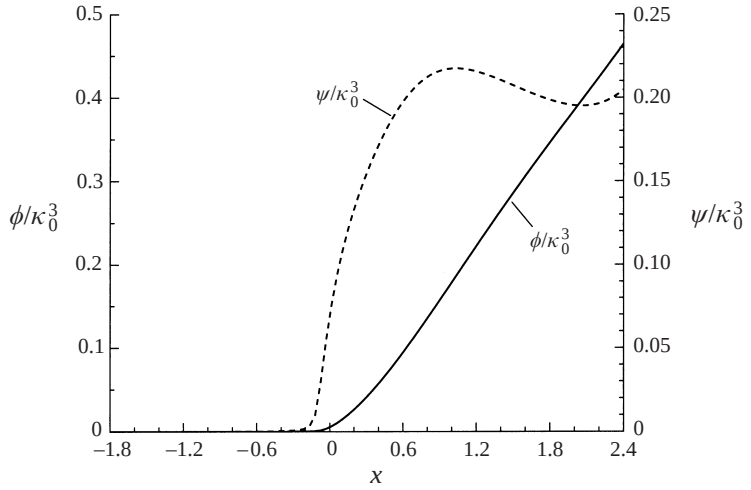

FIGURE 16. A stable cavitating flow solution of the dynamical system (64)–(70) for the scaled variables ϕ and ψ with continuous growth of bubbles along the axis of nozzle 1 under the same conditions specified in figure 6, but taking into account bubble/bubble interactions with interaction parameter $\Lambda = 300$.

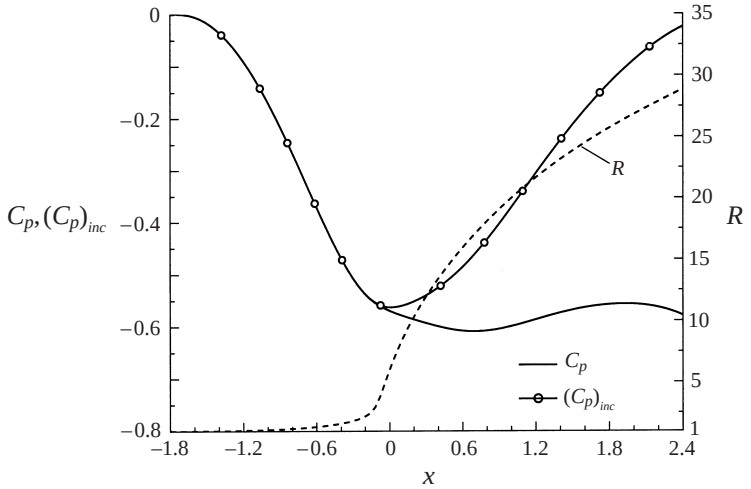

FIGURE 17. Stable cavitating flow distributions of the normalized radius R, the pressure coefficient C_p and its incompressible single-phase value $(C_p)_{inc}$ with continuous growth of bubbles along the axis of nozzle 1 under the same conditions specified in figure 6, but taking into account bubble/bubble interactions with interaction parameter $\Lambda = 300$.

or with a single rebound structure with collapsing bubbles at the nozzle exit. The appropriate value of the interaction parameter Λ corresponding to these solutions can only be determined by comparison with experiments where the same type of behaviour is observed. It can also be demonstrated that bubble/bubble interactions are insignificant (even for values of the interaction parameter Λ of the order of 10^3 to 10^4) for the stable non-cavitating flow solution in nozzle 1 exhibited in figures 3–5. This is, indeed, expected since bubble/bubble interactions can be neglected for small

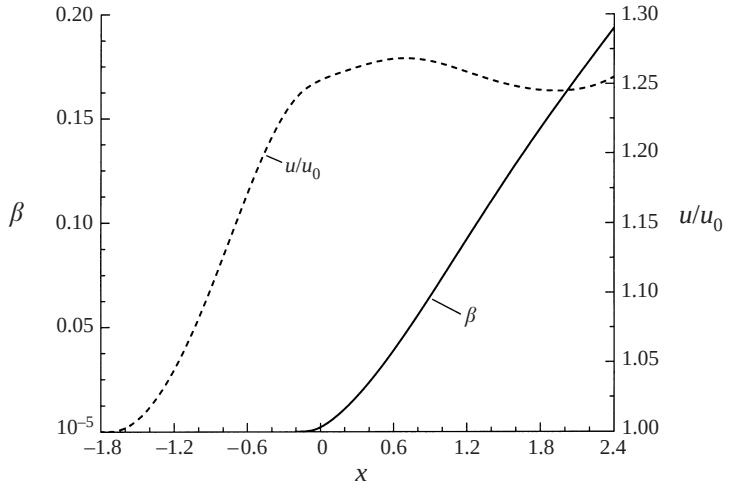

FIGURE 18. Stable cavitating flow distributions of the normalized flow speed u/u_0 and the void fraction β with continuous growth of bubbles along the axis of nozzle 1 under the same conditions specified in figure 6, but taking into account bubble/bubble interactions with interaction parameter $\Lambda = 300$.

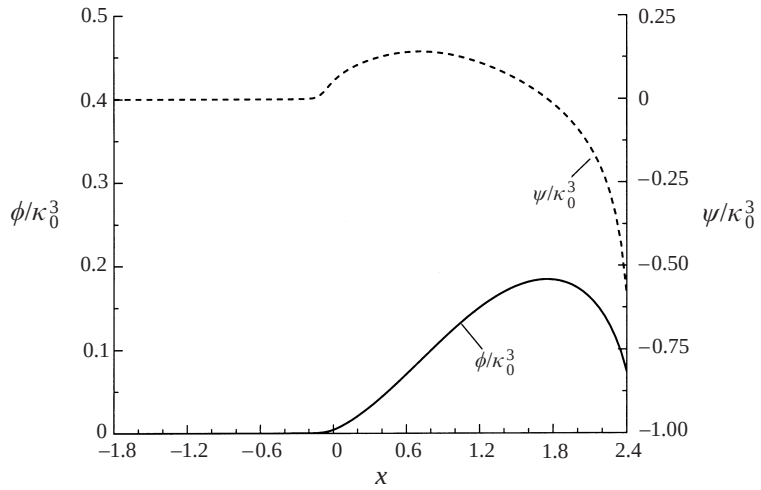

FIGURE 19. A stable cavitating flow solution of the dynamical system (64)–(70) for the scaled variables ϕ and ψ with a single rebound structure (growth followed by collapse of bubbles) along the axis of nozzle 1 under the same conditions specified in figure 6, but taking into account bubble/bubble interactions with interaction parameter $\Lambda = 350$.

bubble sizes with radii of the order of 10 μm with insignificant growth and collapse, as shown in figure 4.

We now discuss the effects of the various damping mechanisms on cavitating nozzle flows in our model. Our calculations show that the effect of thermal damping in the near-isothermal case without bubble/bubble interactions ($k = 1$, $Re_\ell/Re = 1$, finite α and $\Lambda = 1$; see Prosperetti 1991) does not overcome the flashing flow instability of figures 6–8 in nozzle 1. It is also insignificant for the non-cavitating stable solution of figures 3–5. Its only effect is to shift the bifurcation value of the initial value slightly showing that the near-isothermal approximation does not seem to take into

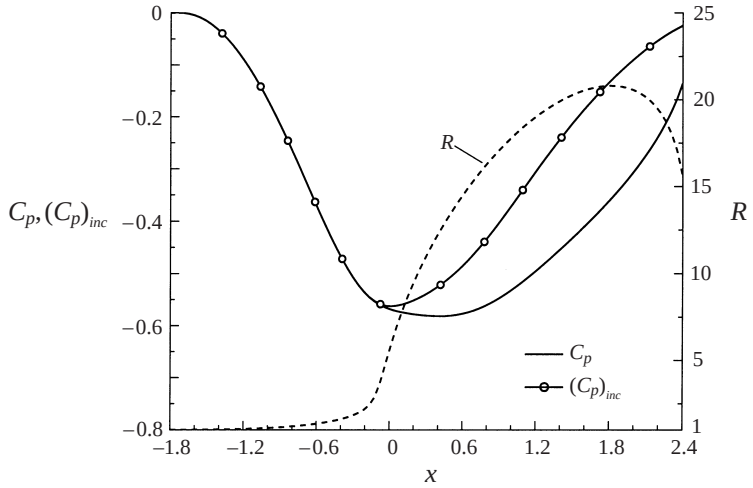

FIGURE 20. Stable cavitating flow distributions of the normalized radius R, the pressure coefficient C_p and its incompressible single-phase value $(C_p)_{inc}$ with a single rebound structure (growth followed by collapse of bubbles) along the axis of nozzle 1 under the same conditions specified in figure 6, but taking into account bubble/bubble interactions with interaction parameter $\Lambda = 350$.

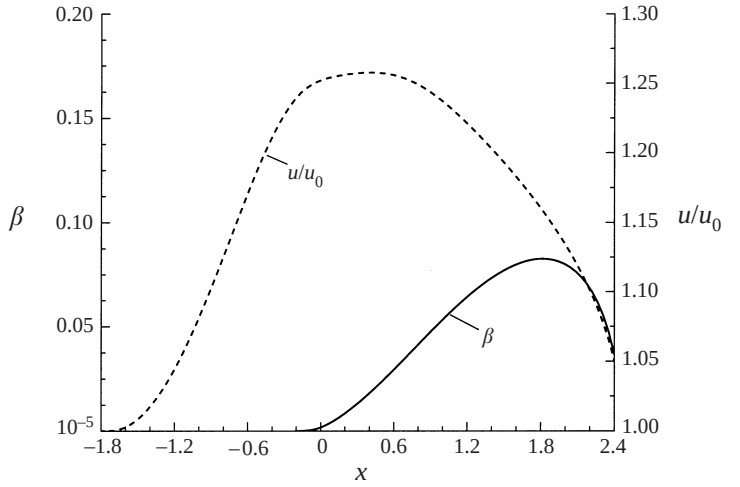

FIGURE 21. Stable cavitating flow distributions of the normalized flow speed u/u_0 and the void fraction β with a single rebound structure (growth followed by collapse of bubbles) along the axis of nozzle 1 under the same conditions specified in figure 6, but taking into account bubble/bubble interactions with interaction parameter $\Lambda = 350$.

account the thermal damping effect satisfactorily (we can, therefore, set $\alpha \to \infty$ and $k \neq 1$ in our model equations). This suggests that in our model equations, we should take into account thermal damping as well as other damping effects by varying the ratio Re_ℓ/Re. As has been demonstrated in figure 15 for nozzle 2, the use of the damping coefficient v'_D alone in our model equations (19)–(23) for various damping mechanisms without bubble/bubble interactions ($\Lambda = 1$) may not lead to a stable cavitating flow solution. Therefore, a stable cavitating nozzle flow solution for the initial-value problem of our model equations (19)–(23) requires, in general, that bubble/bubble interactions should also be taken into account ($\Lambda \gg 1$). For this

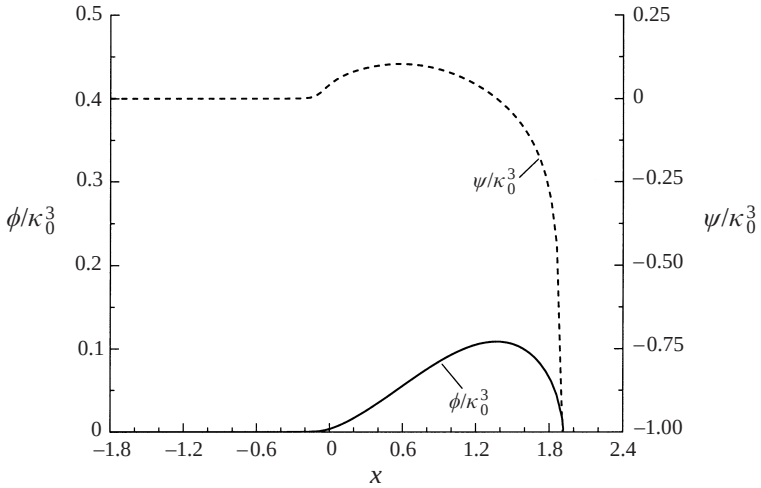

FIGURE 22. Solution of the dynamical system (64)–(70) for the scaled variables ϕ and ψ with bubble collapse instability (corresponding to an unbounded solution) along the axis of nozzle 1 under the same conditions specified in figure 6, but taking into account bubble/bubble interactions with interaction parameter $\Lambda = 400$.

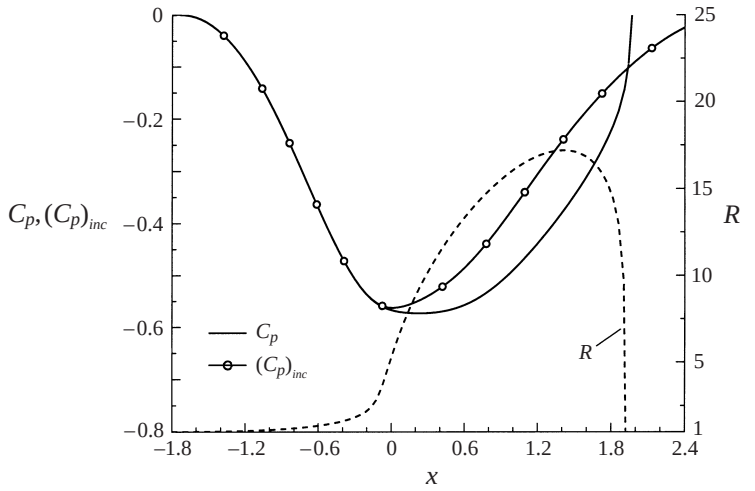

FIGURE 23. Distributions of the normalized radius R, the pressure coefficient C_p and its incompressible single-phase value $(C_p)_{inc}$ with bubble collapse instability (corresponding to an unbounded solution) along the axis of nozzle 1 under the same conditions specified in figure 6, but taking into account bubble/bubble interactions with interaction parameter $\Lambda = 400$.

reason we investigate the various damping effects on the cavitating flow by varying the ratio Re_ℓ/Re for $\Lambda \gg 1$. In particular, we choose to consider the effect of various damping mechanisms on the unstable solution of figures 22–24 for $\Lambda = 400$ by increasing the value of Re_ℓ/Re from unity to 90. The results are shown in figures 25–27. In this case, the instability is inhibited by the various damping mechanisms resulting in a stable cavitating flow solution with collapsing bubbles at the nozzle exit, a structure similar to that exhibited in figures 19–21 for $\Lambda = 350$ and $Re_\ell/Re = 1$. The results demonstrate that the damping effects seem to be as important as those

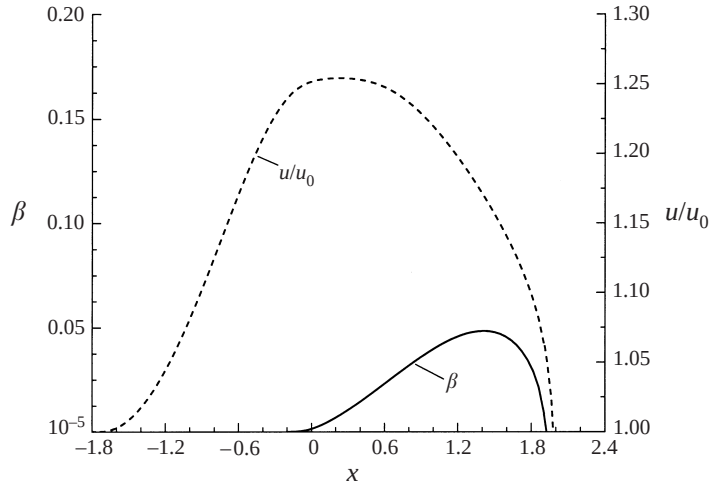

FIGURE 24. Distributions of the normalized flow speed u/u_0 and the void fraction β with bubble collapse instability (corresponding to an unbounded solution) along the axis of nozzle 1 under the same conditions specified in figure 6, but taking into account bubble/bubble interactions with interaction parameter $\Lambda = 400$.

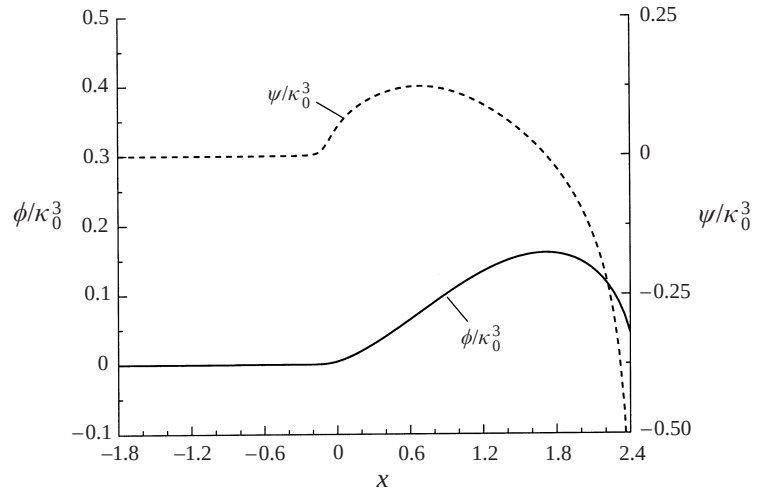

FIGURE 25. A stable cavitating flow solution of the dynamical system (64)–(70) for the scaled variables ϕ and ψ with a single rebound structure (growth followed by collapse of bubbles) along the axis of nozzle 1, obtained with a damping coefficient $Re_\ell/Re = 90$ stabilizing the corresponding bubble collapse instability in figure 22 for the value of the interaction parameter $\Lambda = 400$.

of bubble/bubble interactions in our model equations for cavitating nozzle flows; therefore, both effects should be considered simultaneously (this suggests that we should consider $\Lambda \gg 1$ and $Re_\ell/Re \gg 1$ in our model equations). The appropriate values for Λ and Re_ℓ/Re can only be found in comparison with those experiments showing the same behaviour and with no influence from the back pressure.

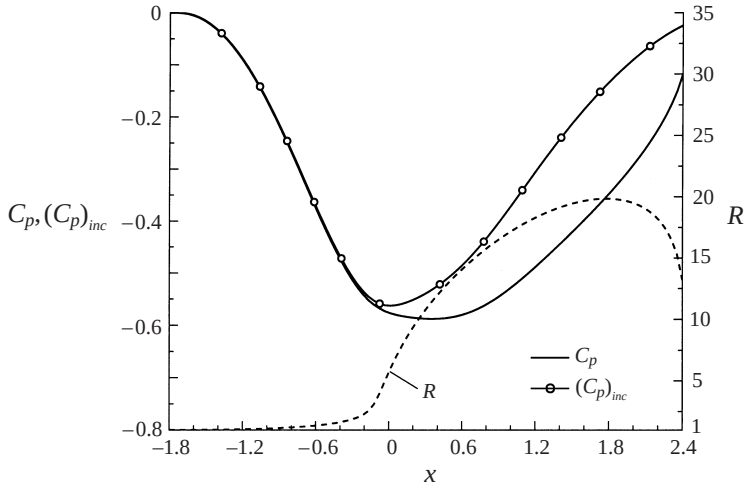

FIGURE 26. Distributions of the normalized radius R, the pressure coefficient C_p and its incompressible single-phase value $(C_p)_{inc}$ with a single rebound structure (growth followed by collapse of bubbles) along the axis of nozzle 1, obtained with a damping coefficient $Re_\ell/Re = 90$ stabilizing the corresponding bubble collapse instability in figure 23 for the value of the interaction parameter $\Lambda = 400$.

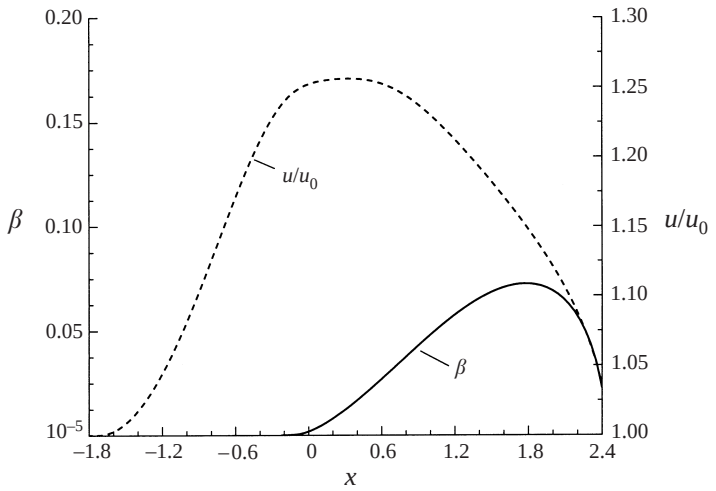

FIGURE 27. Distributions of the normalized flow speed u/u_0 and the void fraction β with a single rebound structure (growth followed by collapse of bubbles) along the axis of nozzle 1, obtained with a damping coefficient $Re_\ell/Re = 90$ stabilizing the corresponding bubble collapse instability in figure 24 for the value of the interaction parameter $\Lambda = 400$.

7. Conclusions

A homogeneous bubbly mixture model, which takes into account bubble/bubble interactions by the local homogeneous model of Kubota *et al.* (1992) and various damping mechanisms, lumped together in the form of viscous dissipation by a damping coefficient, is constructed for quasi-one-dimensional cavitating nozzle flows. The system of equations is uncoupled leading to a nonlinear dynamical system of scaled variables that characterize deviations of the flow speed and its derivatives from their corresponding incompressible single-phase values. The initial-value problem for the dynamical system is then solved for cavitating nozzle flows. Results obtained

when bubble/bubble interactions are neglected show either stable non-cavitating flow solution for which the maximum radius remains smaller than the Blake radius or flashing flow solutions as has recently been found by Wang & Brennen (1997, 1998). Stable steady-state cavitating nozzle flow solutions were found for some range of the bubble/bubble interaction parameter when bubble/bubble interactions were taken into account. These solutions exhibited either a continuous growth of bubbles with evaporating bubbles at the nozzle exit or a single rebound structure with growth of bubbles followed by collapse. A further increase in the bubble/bubble interaction parameter leads to solutions with collapse structure instabilities, which are stabilized by increasing the damping coefficient by orders of magnitude beyond that of viscous damping. The results show that bubble/bubble interactions and damping mechanisms have to be considered simultaneously for stable solutions. The effects of the wall shear stress on cavitating flows and on the flow instabilities were insignificant for all the cases considered.

It is worthwhile to mention that the damping mechanisms (all lumped together in the form of viscous dissipation by a damping coefficient) of this simplified model can only yield an estimate of the relative magnitude of all of the damping effects, with respect to that of viscous damping, for stable steady flows. More sophisticated models, which take into account the various damping mechanisms in a more realistic manner, require the use of the energy equation for cavitating bubbles (e.g. for an improvement on the thermal behaviour, the Prosperetti model (1991) can be used). The problem has to be, then, considered numerically. It should also be mentioned that we only considered the solution of the initial-value problem of the model equations; therefore, other solutions such as choked nozzle flow solutions with shock waves arising from the influence of the back pressure can also be possible.

This work is supported in part by Deutsche Forschungsgemeinschaft Graduiertenkolleg 'Energie- und Umwelttechnik' at the University of Karlsruhe, and in part by the Scientific and Technical Research Council of Turkey (TÜBİTAK) and by the Turkish Academy of Sciences (TÜBA). The authors would also like to thank Professor L. van Wijngaarden, Professor C. E. Brennen, Professor A. Prosperetti, Professor Y. Matsumoto, Professor D. Lohse and Professor R. I. Nigmatulin for many valuable comments and suggestions.

Appendix A. Pressure–velocity relation for quasi-one-dimensional cavitating nozzle flow

The pressure–velocity relation for quasi-one-dimensional cavitating nozzle flow, whose derivation is discussed in § 4, can be written as

$$p_v - p = A_1(u,x)\frac{\mathrm{d}^2u}{\mathrm{d}x^2} + B_1(u,x)\left(\frac{\mathrm{d}u}{\mathrm{d}x}\right)^2 + C_1(u,x)\frac{\mathrm{d}u}{\mathrm{d}x} + D_1(u,x) \tag{A 1}$$

where

$$A_1(u,x) = \frac{L^2\kappa_0^2}{6}\left(\frac{u}{\omega}-1\right)^{-1/3} u\left[2+(3\Lambda^2-1)\left(\frac{u}{\omega}-1\right)\right], \tag{A 2}$$

$$B_1(u,x) = -\frac{L^2\kappa_0^2}{18}\left(\frac{u}{\omega}-1\right)^{-4/3}\frac{u}{\omega}\left[6\Lambda^2-(6\Lambda^2-1)\frac{u}{\omega}\right], \tag{A 3}$$

$$C_1(u,x) = \frac{L^2\kappa_0^2}{18}\left(\frac{u}{\omega}-1\right)^{-4/3}\frac{u}{\omega}\left\{\left[9(1-\Lambda^2)+(30\Lambda^2-12)\frac{u}{\omega}\right.\right.$$
$$\left.\left.-(21\Lambda^2-5)\frac{u^2}{\omega^2}\right]\frac{\mathrm{d}\omega}{\mathrm{d}x}+\frac{24}{L^2(Re)\kappa_0^2}\left(\frac{u}{\omega}-1\right)^{1/3}+\frac{6(\gamma-1)p_{g0}\delta_{k1}}{5\gamma L\kappa_0^6\alpha(u/\omega-1)}\right\} \quad (A\,4)$$

and

$$D_1(u,x) = -\frac{L^2\kappa_0^2}{18}\left(\frac{u}{\omega}-1\right)^{-4/3}\left\{3u\frac{u}{\omega}\left[2+(3\Lambda^2-1)\left(\frac{u}{\omega}-1\right)\right]\left(\frac{u}{\omega}-1\right)\frac{\mathrm{d}^2\omega}{\mathrm{d}x^2}\right.$$
$$+\left(\frac{u}{\omega}\right)^2\left[9(1-\Lambda^2)+(24\Lambda^2-12)\frac{u}{\omega}-(15\Lambda^2-4)\frac{u^2}{\omega^2}\right]\left(\frac{\mathrm{d}\omega}{\mathrm{d}x}\right)^2$$
$$+\left(\frac{u}{\omega}\right)^2\left[\frac{24}{L^2(Re)\kappa_0^2}\left(\frac{u}{\omega}-1\right)^{1/3}+\frac{6(\gamma-1)p_{g0}\delta_{k1}}{5\gamma L\kappa_0^6\alpha(u/\omega-1)}\right]\frac{\mathrm{d}\omega}{\mathrm{d}x}$$
$$\left.-\frac{18\,S_0}{L^2\kappa_0^3}\left(\frac{u}{\omega}-1\right)+\frac{18\,p_{g0}}{L^2\,\kappa_0^{3k+2}\left(u/\omega-1\right)^{k-4/3}}\right\}. \quad (A\,5)$$

Appendix B. Third-order differential equation for the flow speed in quasi-one-dimensional cavitating nozzle flow

The third-order differential equation for the velocity in quasi-one-dimensional cavitating nozzle flow, derived in § 4, is of the form

$$A(u,x)\frac{\mathrm{d}^3u}{\mathrm{d}x^3}+\left[B(u,x)\frac{\mathrm{d}u}{\mathrm{d}x}+C(u,x)\right]\frac{\mathrm{d}^2u}{\mathrm{d}x^2}+D(u,x)\left(\frac{\mathrm{d}u}{\mathrm{d}x}\right)^3$$
$$+E(u,x)\left(\frac{\mathrm{d}u}{\mathrm{d}x}\right)^2+F(u,x)\frac{\mathrm{d}u}{\mathrm{d}x}+G(u,x)=0 \quad (B\,1)$$

where

$$A(u,x)=A_1(u,x)=\frac{L^2\,\kappa_0^2}{6}\left(\frac{u}{\omega}-1\right)^{-1/3}u\left[2+(3\Lambda^2-1)\left(\frac{u}{\omega}-1\right)\right], \quad (B\,2)$$

$$B(u,x)=\frac{\partial A_1}{\partial u}+2B_1(u,x)=\frac{L^2\,\kappa_0^2}{18}\left(\frac{u}{\omega}-1\right)^{-4/3}$$
$$\times\left[(27\Lambda^2-7)\frac{u^2}{\omega^2}-(36\Lambda^2-12)\frac{u}{\omega}+9(\Lambda^2-1)\right], \quad (B\,3)$$

$$C(u,x)=\frac{\partial A_1}{\partial x}+C_1(u,x)+\frac{4}{3(Re_\ell)}=-\frac{L^2\kappa_0^2}{18}\left(\frac{u}{\omega}-1\right)^{-4/3}\frac{u}{\omega}$$
$$\times\left\{\left[(27\Lambda^2-7)\frac{u^2}{\omega^2}-(36\Lambda^2-12)\frac{u}{\omega}+9(\Lambda^2-1)\right]\frac{\mathrm{d}\omega}{\mathrm{d}x}\right.$$
$$\left.-\frac{24}{L^2(Re)\kappa_0^2}\left(\frac{u}{\omega}-1\right)^{1/3}-\frac{6(\gamma-1)p_{g0}\delta_{k1}}{5\gamma L\kappa_0^6\alpha(u/\omega-1)}\right\}+\frac{4}{3(Re_\ell)},\tag{B 4}$$

$$D(u,x)=\frac{\partial B_1}{\partial u}=\frac{L^2\,\kappa_0^2}{27\omega}\left(\frac{u}{\omega}-1\right)^{-7/3}\left[(6\Lambda^2-1)\frac{u^2}{\omega^2}-(15\Lambda^2-3)\frac{u}{\omega}+9\Lambda^2\right],\tag{B 5}$$

$$E(u,x)=\frac{\partial B_1}{\partial x}+\frac{\partial C_1}{\partial u}=-\frac{L^2\kappa_0^2}{54\omega}\left(\frac{u}{\omega}-1\right)^{-7/3}$$
$$\times\left\{\left[(117\Lambda^2-27)\frac{u^3}{\omega^3}-(279\Lambda^2-75)\frac{u^2}{\omega^2}+(189\Lambda^2-63)\frac{u}{\omega}-27(\Lambda^2-1)\right]\frac{\mathrm{d}\omega}{\mathrm{d}x}\right.$$
$$\left.+\frac{72}{L^2(Re)\kappa_0^2}\left(\frac{u}{\omega}-1\right)^{1/3}+\frac{6(\gamma-1)p_{g0}\delta_{k1}}{5\gamma L\kappa_0^6\alpha(u/\omega-1)}\left(4\frac{u}{\omega}+3\right)\right\},\tag{B 6}$$

$$F(u,x)=\frac{\partial C_1}{\partial x}+\frac{\partial D_1}{\partial u}-\omega=\frac{L^2\kappa_0^2}{54\omega}\left(\frac{u}{\omega}-1\right)^{-7/3}$$
$$\times\left\{3u\left(\frac{u}{\omega}-1\right)\left[-(45\Lambda^2-13)\frac{u^2}{\omega^2}+(72\Lambda^2-36)\frac{u}{\omega}-27(\Lambda^2-1)\right]\frac{\mathrm{d}^2\omega}{\mathrm{d}x^2}+\frac{u}{\omega}\right.$$
$$\times\left[(225\Lambda^2-57)\frac{u^3}{\omega^3}-(549\Lambda^2-177)\frac{u^2}{\omega^2}+(405\Lambda^2-189)\frac{u}{\omega}-81(\Lambda^2-1)\right]\left(\frac{\mathrm{d}\omega}{\mathrm{d}x}\right)^2$$
$$+\left[\frac{72}{L^2(Re)\kappa_0^2}\left(\frac{u}{\omega}-1\right)^{1/3}\frac{u}{\omega}\left(3-\frac{u}{\omega}\right)+\frac{6(\gamma-1)p_{g0}\delta_{k1}}{5\gamma L\kappa_0^6\alpha(u/\omega-1)}\frac{u}{\omega}\left(5\frac{u}{\omega}+9\right)\right]\frac{\mathrm{d}\omega}{\mathrm{d}x}$$
$$\left.-\frac{18S_0}{L^2\kappa_0^3}\left(\frac{u}{\omega}-1\right)+\frac{54kp_{g0}}{L^2\kappa_0^{3k+2}\left(u/\omega-1\right)^{k-4/3}}\right\}-\omega,\tag{B 7}$$

$$G(u,x)=\frac{\partial D_1}{\partial x}-\left(\frac{\mathrm{d}p_v}{\mathrm{d}x}+\varphi\omega uC_w\right)=-\frac{L^2\kappa_0^2}{54\omega}\left(\frac{u}{\omega}-1\right)^{-7/3}\frac{u}{\omega}$$
$$\times\left\{9u\omega\left[2+(3\Lambda^2-1)\left(\frac{u}{\omega}-1\right)\right]\left(\frac{u}{\omega}-1\right)^2\frac{\mathrm{d}^3\omega}{\mathrm{d}x^3}\right.$$
$$+3u\left(\frac{u}{\omega}-1\right)\left(\left[-(45\Lambda^2-13)\frac{u^2}{\omega^2}+(72\Lambda^2-36)\frac{u}{\omega}-27(\Lambda^2-1)\right]\frac{\mathrm{d}\omega}{\mathrm{d}x}\right.$$
$$+\frac{24}{L^2(Re)\kappa_0^2}\left(\frac{u}{\omega}-1\right)^{1/3}+\left.\frac{6(\gamma-1)p_{g0}\delta_{k1}}{5\gamma L\kappa_0^6\alpha(u/\omega-1)}\right)\frac{\mathrm{d}^2\omega}{\mathrm{d}x^2}+2\frac{u}{\omega}$$
$$\times\left[(60\Lambda^2-16)\frac{u^3}{\omega^3}-(150\Lambda^2-54)\frac{u^2}{\omega^2}+(117\Lambda^2-63)\frac{u}{\omega}-27(\Lambda^2-1)\right]\left(\frac{\mathrm{d}\omega}{\mathrm{d}x}\right)^3$$
$$+\frac{u}{\omega}\left[\frac{72}{L^2(Re)\kappa_0^2}\left(\frac{u}{\omega}-1\right)^{1/3}\left(2-\frac{u}{\omega}\right)+\frac{6(\gamma-1)p_{g0}\delta_{k1}}{5\gamma L\kappa_0^6\alpha(u/\omega-1)}\left(\frac{u}{\omega}+6\right)\right]\left(\frac{\mathrm{d}\omega}{\mathrm{d}x}\right)^2$$
$$\left.-\frac{18S_0}{L^2\kappa_0^3}\left(\frac{u}{\omega}-1\right)\frac{\mathrm{d}\omega}{\mathrm{d}x}+\frac{54kp_{g0}}{L^2\kappa_0^{3k+2}\left(u/\omega-1\right)^{k-4/3}}\frac{\mathrm{d}\omega}{\mathrm{d}x}\right\}-\left(\frac{\mathrm{d}p_v}{\mathrm{d}x}+\varphi\omega uC_w\right).\tag{B 8}$$

Appendix C. Existence of instabilities of the classical Rayleigh–Plesset equation for bubble dynamics in cavitating nozzle flow

We, herein, demonstrate the existence of instabilities of the model equations (19)–(23) for $\Lambda = 1$ (nozzle flow equations coupled to the classical Rayleigh–Plesset equation for spherical bubble dynamics). For this reason, we first consider the Blake stability for mechanical equilibrium. Since all bubbles at the nozzle inlet with radii R_0' are assumed to be in mechanical equilibrium, it follows from the classical Rayleigh–Plesset equation that this equilibrium state is stable if $R_0' < R_B'$ and, otherwise, unstable where R_B' is the Blake radius defined by (for details see, e.g. Brennen 1995)

$$R_B' = \left[\frac{3kR_0'^3 p_{g0}'}{2S'}\right]^{1/2}. \tag{C 1}$$

This equilibrium stability condition can be stated as

$$R_B \equiv \frac{R_B'}{R_0'} = \tfrac{1}{2}\left[k(12 + 3\sigma_0 We_{R0})\right]^{1/2} > 1. \tag{C 2}$$

Since σ_0 and We_{R0} are both positive and $k \geqslant 1$, it follows that the equilibrium state at the nozzle inlet is a stable one. We can now extend this equilibrium stability condition to apply locally at any location along the nozzle axis. Let R_E' be a fictitious bubble radius (with $\mathrm{d}R_E'/\mathrm{d}t' = \mathrm{d}^2R_E'/\mathrm{d}t'^2 = 0$) defined by the local equilibrium condition

$$p_v' - p' + p_g' - \frac{2S'}{R_E'} = 0 \tag{C 3}$$

at any location along the nozzle axis (this implies that $p_v' + p_g' > p'$, which presumably holds for cavitating flows). Consider a fictitious change of state where the gas expands from this fictitious local equilibrium state polytropically according to $p_g'(R_E'/R')^{3k}$ with constant mass holding p_v' and p' fixed at their local values for an arbitrarily small virtual variation of the bubble radius

$$R' = R_E'(1 + \xi) \tag{C 4}$$

with $|\xi| \ll 1$. Now by substituting for R' from (C4) into the Rayleigh–Plesset equation (6) with $v_D' = v_\ell'$ and by using (C3) (e.g. see Brennen 1995, chapter 2), we obtain for small values of ξ

$$R'\frac{\mathrm{d}^2R'}{\mathrm{d}t'^2} + \frac{3}{2}\left(\frac{\mathrm{d}R'}{\mathrm{d}t'}\right)^2 + \frac{4v_\ell'}{R'}\frac{\mathrm{d}R'}{\mathrm{d}t'} = \frac{\xi}{\rho_\ell'}\left[\frac{2S'}{R_E'} - 3kp_g'\right]. \tag{C 5}$$

The right-hand side has the opposite sign as ξ if

$$p_g' > \frac{2S'}{3kR_E'}, \tag{C 6}$$

which is the condition for local equilibrium stability. Now the real bubble radius R' at this fixed location of the nozzle, attained by the nozzle area variation, can deviate only slightly from the fictitious local equilibrium value R_E' if local stability is to be satisfied (otherwise, the flow field will be locally unstable). Therefore, the local stability condition can be approximated by

$$p_g' > \frac{2S'}{3kR'}. \tag{C 7}$$

Substituting for p'_g from $p'_g = p'_{g0}(R'_0/R')^{3k}$, we obtain the local stability condition

$$R < \left(\frac{3kp'_{g0}R'_0}{2S'}\right)^{1/(3k-1)} = R_B^{2/(3k-1)}, \tag{C 8}$$

where R_B is given by (C2). For isothermal flow ($k = 1$), (C8) reduces to the Blake stability condition

$$R < R_B. \tag{C 9}$$

REFERENCES

Biesheuvel, A. & Wijngaarden, L. van 1984 Two-phase flow equations for a dilute dispersion of gas bubbles in liquid. *J. Fluid Mech.* **148**, 301–318.

Blake, J. R. & Gibson, D. C. 1987 Cavitation bubbles near boundaries. *Ann. Rev. Fluid Mech.* **19**, 99–123.

Brennen, C. E. 1995 *Cavitation and Bubble Dynamics*. Oxford University Press.

Chahine, G. L. & Duraiswami, R. 1992 Dynamical interactions in a multi-bubble cloud. *Trans. ASME* I: *J. Fluids Engng* **114**, 680–686.

Chapman, R. & Plesset, M. 1971 Thermal effects in the free oscillation of gas bubbles. *Trans. ASME* D: *J. Basic Engng* **93**, 373–376.

Colonius, T., Brennen, C. E. & d'Auria, F. 1998 Computation of shock waves in cavitating flows. In *Proc. FED98, ASME/FED Third International Symposium on Numerical Methods in Multiphase Flow, 21–26 June 1998, Washington DC*, Paper no. FEDSM98-507.

Delale, C. F. & Schnerr, G. H. 1998 Quasi-one-dimensional cavitating nozzle flows. Presented at the Third International Conference on Multiphase Flow (ICMF'98) 8–12 June 1998, Lyon.

Hammitt, F. G. 1980 *Cavitation and Multiphase Flow Phenomena*. McGraw-Hill.

Ishii, R., Umeda, Y., Murata, S. and Shishido, N. 1993 Bubbly flows through a converging–diverging nozzle. *Phys. Fluids* A **5**, 1630–1643.

Kameda, M. & Matsumoto, Y. 1995 Structure of shock waves in a liquid containing gas bubbles. In *IUTAM Symposium on Waves in Liquid/Gas and Liquid/Vapour Two-Phase Systems*, pp. 117–126. Kluwer.

Knapp, R. T., Daily, J. W. & Hammitt, F. G. 1970 *Cavitation*. McGraw-Hill.

Kubota, A., Kato, H. & Yamaguchi, H. 1992 A numerical study of unsteady cavitation on a hydraulic section. *J. Fluid Mech.* **240**, 59–96.

Laufer, J. 1950 Some recent measurements in a two-dimensional turbulent channel. *J. Aeronat. Sci.* **17**, 277–287.

Miksis, M. J. & Ting, L. 1984 Nonlinear radial oscillations of a gas bubble including thermal effects. *J. Acoust. Soc. Am.* **76**, 897–905.

Miksis, M. J. & Ting, L. 1987 A numerical study of thermal effects on nonlinear bubble oscillations. *J. Acoust. Soc. Am.* **81**, 1331–1340.

Nigmatulin, R. I., Khabeev, N. S. & Nagiev, F. B. 1981 Dynamics, heat and mass transfer of vapor-gas bubbles in a liquid. *Intl J. Heat Mass Transfer* **24**, 1033–1044.

Noordzij, L. & van Wijngaarden, L. 1974 Relaxation effects, caused by the relative motion, on shock waves in gas-bubble/liquid mixtures. *J. Fluid Mech.* **66**, 115–143.

Prosperetti, A. 1991 The thermal behaviour of oscillating gas bubbles. *J. Fluid Mech.* **222**, 587–616.

Prosperetti, A. Crum, L. A. & Commander, K. W. 1988 Nonlinear bubble dynamics. *J. Acoust. Soc. Am.* **83**, 502–514.

Prosperetti, A. & Lezzi, A. 1986 Bubble dynamics in a compressible liquid. Part 1. First-order theory. *J. Fluid Mech.* **168**, 457–478.

Schnerr, G. H., Adam, S., Lanzenberger, K. & Schulz, R. 1995 Multiphase flows: condensation and cavitation problems. In *Computational Fluid Dynamics Review 1* (ed. M. Hafez & K. Oshima). John Wiley.

Schulz, R. 1995 Entwicklung eines numerischen Verfahrens zur Simulation von Wolkenkavitation. PhD Thesis, University of Karlsruhe (TH), Germany. VDI-Verlag GmbH, Düsseldorf, Reihe 7, Nr. 274 .

Tangren, R. F., Dodge, C. H. & Seifert, H. S. 1949 Compressibility effects in two-phase flow. *J. Appl. Phys.* **20**, 637–645.

Wallis, G. B. 1969 *One-Dimensional Two-Phase Flow*. McGraw-Hill.

Wang, Y. C. & Brennen, C. E. 1997 One-dimensional bubbly cavitating flows through a converging–diverging nozzle. Presented at the 1997 ASME Fluids Engineering Meeting in Vancouver.

Wang, Y. C. & Brennen, C. E. 1998 One-dimensional bubbly cavitating flows through a converging–diverging nozzle. *Trans. ASME* I: *J. Fluids Engng* **120**, 166–170.

Ward-Smith, A. J. 1980 *Internal Fluid Flow*, p. 186. Clarendon Press.

Watanabe, M. & Prosperetti, A. 1994 Shock waves in dilute bubbly liquids. *J. Fluid Mech.* **274**, 349–381.

Wijngaarden L. van 1968 On the equations of motion for mixtures of liquid and gas bubbles. *J. Fluid Mech.* **33**, 465–474.

Wijngaarden, L. van 1972 One-dimensional flow of liquids containing small gas bubbles. *Ann. Rev. Fluid. Mech.* **4**, 369–396.

Young, F. R. 1989 *Cavitation*. McGraw-Hill.